HØGSKOLEN I OSLO
OG AKERSHUS

PROSJEKT NR: 1817

TILGJENGELIGHET

**Institutt for maskin, elektronikk og kjemi**
Postadresse: Postboks 4 St. Olavs plass, 0130 Oslo
Besøksadresse: Pilestredet 35, Oslo

Telefon: 67 23 50 00
E-post: post@hioa.no

# BACHELOROPPGAVE

| BACHELOROPPGAVENS TITTEL | DATO |
|---|---|
| CW fNIRS with short channel regression and amplitude modulation | 23.05.18 |
| | ANTALL SIDER/BILAG<br>83 / 27 |
| FORFATTER(E)<br>S300980 - Max Engvik<br>S300331 - Marte Helén Andersen Gjestemoen<br>S237428 - Anders Horpestad<br>S899855 - Janne Martinsen<br>S237539 - Stian Nordli | INTERN VEILEDER<br>Peyman Mirtaheri |

| UTFØRT I SAMARBEID MED | EKSTERN(E) VEILEDER(E) |
|---|---|
| Peyman Mirtaheri | |

SAMMENDRAG

Functional Near Infrared Spectroscopy (fNIRS) is a relatively new and promising field within brain imaging and neuroscience. It offers a cost efficient, non-invasive method for brain studies, both for research and clinical purposes. Based on existing NIRS technologies, fNIRS uses near infrared light to measure the presence of different chromophores in the brain.

Recent studies have explored the possibility of using data from a short separation channel as a basis for regression filtering to remove noise generated by the superficial layers of the head, but faces a challenge as the short channel quickly saturates.

This report describes the process of making a working fNIRS instrument with both a short- and a long-channel, which measures changes in the amount of hemoglobin in the brain during cognitive tasks. It does so by detecting the attenuation of NIR light travelling from the emission source, through the brain and to a detector. The goal is to overcome short channel saturation challenges by using an amplitude modulated signal.

The technology of NIRS and fNIRS is accounted for, as well as theory related to light and its behavior in human tissue. The modified Beer-Lambert law, which must be applied to continuous wave (CW) fNIRS data to calculate the relative concentration of chromophores in the blood, is explained. The anatomy of the skin and the human brain is accounted for, as well as physiological processes related to neural activity in the brain.

The circuit design of the instrument is thoroughly explained, as efforts have been made to overcome the hardware challenges posed by implementing a short distance (1 cm) between light source and detector. Instrument design and functionality was tested by performing blood flow restriction tests and cognitive tests on several subjects. The data was read and pre-processed in a graphical user interface programmed in MATLAB. Final data analyses were compared to earlier studies and showed that the instrument works as expected.

The fNIRS instrument described in this report is meant to accommodate the need for precise, low-noise measurements of hemodynamic responses in the brain, and facilitate further research of short-channel regression filtering in fNIRS.

| |
|---|
| fNIRS |
| Short separation channel |
| Electronics |

# Preface

This thesis marks the end of the group's three-year long bachelor study as electronics engineers at OsloMet – metropolitan university. This thesis documents the work we have put into our bachelor project in the spring of 2018.

The group has overcome many challenges this semester and through them learned and grown a lot.
We are proud of what we have achieved.

This thesis is mainly written with the grader in mind, but also whoever might find an interest in this document. The purpose of this document is to give an insight in the theory, process and validation of the product we have made.

As a start we would like to give a big thank you to everyone who has helped us during this project:
Morten Ødegård for always doing his uttermost to help us whenever we needed it.
Halvard Fredly for excellent help with finding and acquiring components.
Frode Flem for helping us when we had a proper electronics pinch.
Philip Wigglesworth for giving us guidelines on how to validate our system.
And last, but certainly not least, Peyman Mirtaheri for continuous guidance throughout the whole semester.

# Table of content

# List of figures

## List of Tables

## List of Symbols

| Symbol | Explanation | Unit or constant value |
|---|---|---|
| [X] | Concentration of absorbing species | |
| $\Delta$ | Delta, change of a variable quantity | |
| A | Amplification | |
| $A_l$ | Absorbance | |
| B | Bandwidth | Hertz [Hz] |
| $C_f$ | Parasitic feedback capacitance | Farad [F] |
| d | Distance | Meter [m] |
| DPF | Concentration of chromophores | |
| e | Electron charge | $1.602 \cdot 10^{-19}$ C |
| $e_n$ | Johnson noise voltage | V/$\sqrt{}$Hz |
| $\varepsilon$ | Molar extinction coefficient | |
| f | Frequency | Hertz [Hz] |
| G | Scattering dependent light intensity loss parameter | |
| GBP | Gain-Bandwidth Product | Hertz [Hz] |
| $HbO_2$ | Oxygenated hemoglobin | |
| HbR | Deoxygenated hemoglobin | |
| $i^2_n$ | Current noise power spectral density | |
| $I_E$ | Current | Ampere [A] |
| $I_l$ | Intensity | |
| k | Boltzman constant | $1.38 \cdot 10^{-23}$ J/K |
| L | Pathlength | Meter [m] |
| n | Any integer | |
| OD | Optical density (or absorption) | |
| OPL | Optical pathlength | |
| R | Resistance | Ohm [Ω] |
| $SO_2$ | Blood oxygen saturation | |
| T | Absolute temperature | Kelvin [K] |
| t | Time | Second [s] |
| tHb | Total hemoglobin | |
| $t_l$ | Turbidity | |
| V | Voltage | Volt [V] |
| $x_l$ | Thickness | Meter [m] |
| z | Penetration depth | Meter [m] |
| $\beta$ | Beta, transistor's current gain (a.k.a. $h_{FE}$) | |
| $\lambda$ | Wavelength | Meter [m] |
| $\mu_a$ | Absorbing coefficient | |
| $\mu_s$ | Scattering coefficient | |
| $\tau$ | Tau, time constant (a.k.a. transient response) | Second [s] |

## Abbreviations

| | |
|---|---|
| AC | Alternating Current |
| ADC | Analog-to-digital converter |
| ATP | Adenosine Triphosphate |
| BA | Brodmann Area |
| BJT | Bipolar Junction Transistor |
| BOLD | Blood-Oxygen-Level Dependent |
| BPF | Band pass filter |
| CBF | Cerebral Blood Flow |
| CPU | Central Processing Unit |
| CW | Continuous Wave |
| DAC | Digital-to-analog converter |
| DC | Direct Current |
| EDBG | Embedded Debugger |
| EEG | Electroencephalography |
| FD | Frequency domain |
| fMRI | Functional Magnetic Resonance Imaging |
| fNIRI | Functional Near Infrared Imaging |
| fNIRS | Functional Near Infrared Spectroscopy |
| FSV | Full Scale Voltage |
| GUI | Graphical User Interface |
| $HbO_2$ | Oxygenated hemoglobin |
| HbR | Deoxygenated hemoglobin |
| HPF | High pass filter |
| I/O | Input/output |
| IC | Integrated Circuit |
| IDE | Integrated Development Environment |
| LD | Laser diode |
| LED | Light Emitting Diode |
| LPF | Low pass filter |
| LT | Latency Time (for flow to return to baseline levels) |
| MBLL | Modified Beer-Lambert Law |
| MCU | Microcontroller Unit |
| NPN | Negative-Positive-Negative |
| PNP | Positive-negative-positive |
| Opamp | Operational amplifier |
| PACER | Patient-Centric Engineering in Rehabilitation |
| PCB | Printed Circuit Board |
| PET | Positron Emission Tomography |
| PORH | Post Occlusive Reactive Hyperemia |
| RC | Resistor-Capacitor |
| S-D | Source-Detector |
| SS | Short Separation |
| SSC | Short Separation Channel |
| TD | Time Domain |
| TIA | Transimpedance Amplifier |
| TPSF | Temporal Point Spread Function |
| UART | Universal Asynchronous Receiver-Transmitter |
| USB | Universal Serial Bus |

## Abstract

Functional Near Infrared Spectroscopy (fNIRS) is a relatively new and promising field within brain imaging and neuroscience. It offers a cost efficient, non-invasive method for brain studies, both for research and clinical purposes. Based on existing NIRS technologies, fNIRS uses near infrared light to measure the presence of different chromophores in the brain.

Recent studies have explored the possibility of using data from a short separation channel as a basis for regression filtering to remove noise generated by the superficial layers of the head, but faces a challenge as the short channel quickly saturates.

This report describes the process of making a working fNIRS instrument with both a short- and a long-channel, which measures changes in the amount of hemoglobin in the brain during cognitive tasks. It does so by detecting the attenuation of NIR light travelling from the emission source, through the brain and to a detector. The goal is to overcome short channel saturation challenges by using an amplitude modulated signal.

The technology of NIRS and fNIRS is accounted for, as well as theory related to light and its behavior in human tissue. The modified Beer-Lambert law, which must be applied to continuous wave (CW) fNIRS data to calculate the relative concentration of chromophores in the blood, is explained. The anatomy of the skin and the human brain is accounted for, as well as physiological processes related to neural activity in the brain.

The circuit design of the instrument is thoroughly explained, as efforts have been made to overcome the hardware challenges posed by implementing a short distance (1 cm) between light source and detector. Instrument design and functionality was tested by performing blood flow restriction tests and cognitive tests on several subjects. The data was read and pre-processed in a graphical user interface programmed in MATLAB. Final data analyses were compared to earlier studies and showed that the instrument works as expected.

The fNIRS instrument described in this report is meant to accommodate the need for precise, low-noise measurements of hemodynamic responses in the brain, and facilitate further research of short-channel regression filtering in fNIRS.

# 1 Introduction

This thesis is about the development of a portable instrument for use in functional Near-Infrared Spectroscopy (fNIRS). It is based on the concept pioneered by Jöbsis, who in 1977 was the first to show that cerebral oxygenation can be monitored continuously and non-invasively (Jobsis, 1977).

One challenge present in fNIRS today is the noise introduced to the NIRS signal by the extracellular boundaries of the head. In an effort to try to remove this noise, some research groups have implemented a short-separation-channel (SSC) (Gagnon et al., 2011; Koenraadt, Roelofsen, Duysens, & Keijsers, 2014; Scarpa et al., 2013) and used it to regress the short separation (SS) signal from that of the standard channel (Brigadoi & Cooper, 2015). This method has shown some hardware challenges, mainly that the short distance between the source and detector, can cause saturation.

NIRS is a relatively new, non-invasive method of monitoring tissue hemodynamics and oxidative metabolism. Today fNIRS is used as a research tool in neuroscience and shows promises as an alternative or addition to functional Magnetic Resonance Imaging (fMRI), which is the "gold standard" in neuroscientific research. Some of the advantages fNIRS holds over fMRI is:

- The equipment is low-cost
- Small
- Bed-side applicable
- Can be made portable
- Is in general less restraining and therefore makes it possible to conduct brain activation studies in clinical offices and under more realistic conditions.
- Is usable for subjects who cannot use fMRI, e.g. are not able to stay sufficiently still.

This thesis will mainly focus on the development of an instrument which tries to overcome saturation problems on the short channel by modulating the intensity of the NIR light emission source, but some measurements and analysis will also be conducted.

# 2 Background and motivation

The optical laboratory, led by Associate Professor Peyman Mirtaheri, at OsloMet has the vision to develop wireless sensors for biological and medical use. Peyman was given a research grant in 2018 to develop the Patient-Centric Engineering in Rehabilitation (PACER)-Project which aims at "making a device that facilitates an optimized and personalized rehabilitation environment for amputates" (Mirtaheri, 2018). A part of this project will consist of neurological research on amputees in collaboration with the Motion Analysis Lab at OsloMet. It is this part of the project we have been given the task to contribute to.

The title for the bachelor thesis is: "*CW fNIRS with amplitude modulation and short-channel regression*".

## 2.1 Project goal

The goal of this project is to develop an instrument that can be used for functional Near Infrared Spectroscopy (fNIRS) with the following specifications:

- 3 near-infrared (NIR) light sources of different wavelengths; one before, one after and one in the middle of the isosbestic area.
- 2 sensors; short and long channel
- Amplitude modulation of the NIR light intensity signal
- Portable
- Wearable
- Be able to record the NIRS data

Besides this, no other specifications or limitations were given.

The results and system validation will be discussed and presented in a project report, together with a basis of theory and description of materials and methods used to develop and validate the instrument.

### 2.1.1 Procedures

To reach the goal set by this project, the following procedures will be followed. A Gantt chart that shows the procedures over the course of time will follow below.

1. Literature review
2. Circuit research
3. Order necessary parts for the circuits
4. Circuit prototyping and preliminary development
5. Prototype testing
6. PCB development of prototyped circuits

7. PCB tests
8. Test protocol development
9. Preliminary tests
10. Software development
11. Completion of test protocols
12. Integration of circuits and software
13. Conduct tests
14. Report writing (The group will have made notes and written parts continuously during the project)
15. Further development of software algorithms
16. Organize and control tests
17. Finish report revision 1
18. Let supervisor control report
19. Finish report revision 2
20. Proof reading of report
21. Corrections and finish report
22. Make poster and video
23. Hand in poster, report and video
24. Plan bachelors presentation
25. Perform bachelors presentation

### 2.1.2 Gantt chart

*Table 1: Gantt chart*

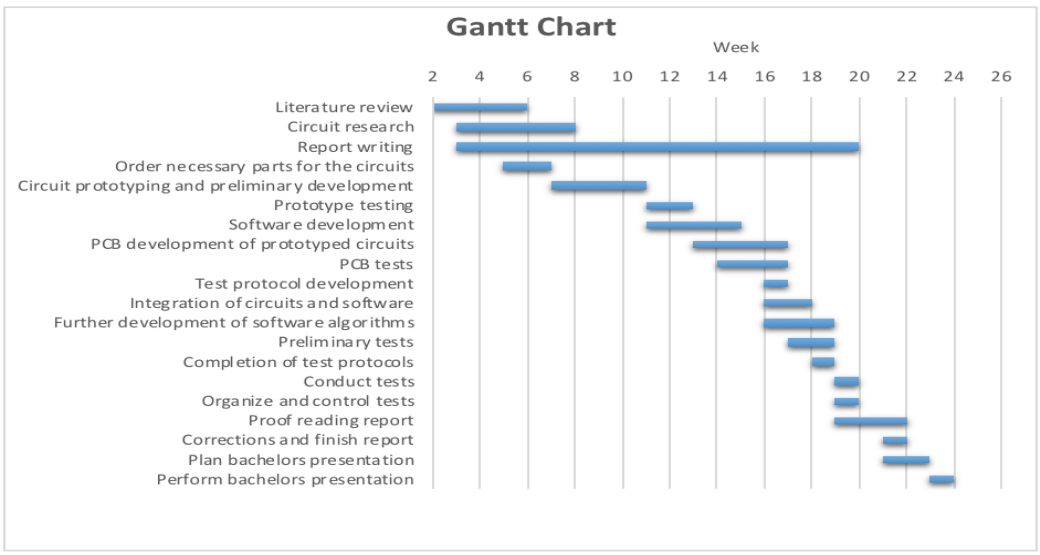

## 2.2 State of the technology

The use of near infrared light for monitoring of cerebral oxygenation started in 1977 when Jöbsis showed that the cerebral cortex was transparent enough to allow NIR light to propagate through it by scattering. In the 1980s and 1990s, the understanding of the physiology of the NIRS signal was in focus, and in 1988 Delpy et. al. developed a mathematical way to take the light scattering into account, and relate the NIRS signal to relative oxygenation levels (Delpy et al., 1988).

In 1993, four different groups successfully used NIRS to measure brain activation. These first measurements were carried out with simple instruments that measured at only a few locations at a time. The next major step was to design instruments that could cover a larger area of the head, allowing topographic mapping of the brain (Scholkmann et al., 2014).

In the 2000s, design of imaging instruments for brain activity mapping was the main focus, making use of fNIRS for Near-Infrared Imaging (fNIRI) (von Lühmann, Herff, Heger, & Schultz, 2015).

Today NIRx is one of the world leading companies developing and producing fNIRS systems. Their "NIRSCOUT" system can monitor the whole cerebral cortex and is capable of both short-distance and multi-distance measurements (NIRx, n.d.). They also produce a fully portable, battery driven and wireless fNIRS system called NIRSport.

The fNIRS technology shows great promise for the future:

> "(…) the emerging use of fNIRS methodologies is likely to represent a drawing power in a variety of challenging experimental and medical contexts; we expect in the near future an increasing use of wireless fNIRS devices, especially in children as well as in specific clinical populations." (Cutini & Brigadoi, 2014, p. 155).

Figure 1 shows a timeline with significant dates in the history of fNIRS.

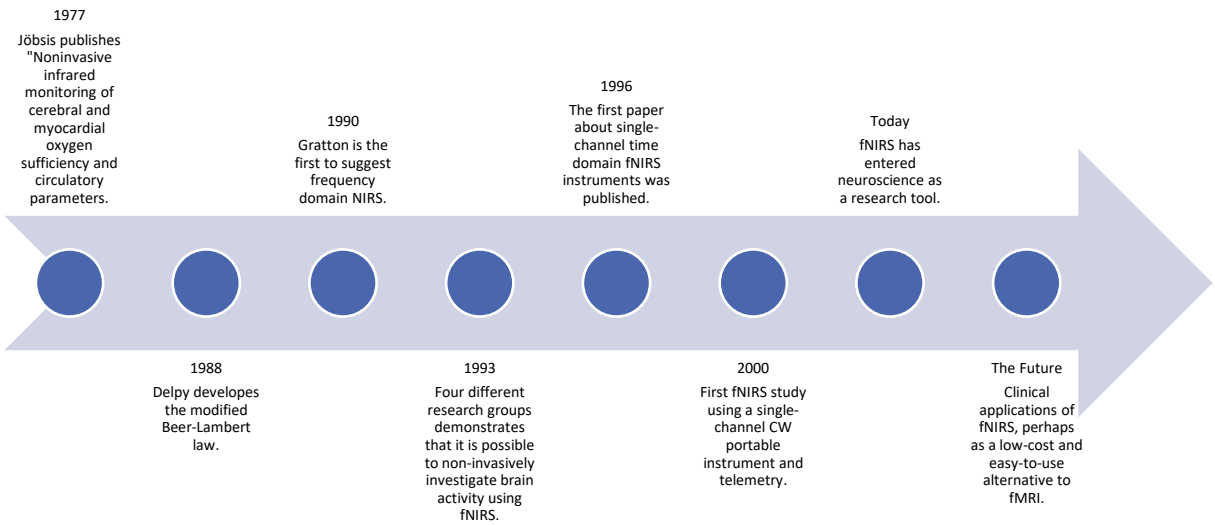


*Figure 1: fNIRS Timeline*

# 3 Theory

## 3.1 NIR

In this chapter NIRS and fNIRS technologies will be explained, in addition to the theory that support them. NIRS will first be explained in a theoretical light, followed by a discussion of its applications. Subsequently the fNIRS technology will be accounted for, touching also upon the challenges related to this field.

### 3.1.1 NIRS

Near infrared spectroscopy (NIRS) is a method that uses near infrared light (700 nm to 1500 nm) to measure percentages of certain substances in a sample, for example water- or fat percentages, or like in clinical applications where NIRS is mainly used to measure the amount of oxy- and deoxyhemoglobin. Measurements are done locally, and a layer of mathematical calculations are applied to determine the absorption, and hence, the percentage of the substance one is interested in measuring. Since NIRS is non-invasive, cheap and easily portable, it shows great promise in a range of research and clinical applications and can be used where other modalities like MRI or PET is not an option (Herold et al., 2017). Because of the low relative power (milliwatts) usually used in near infrared spectroscopy, there has not been shown any negative effects when used on humans or animals (Bozkurt & Onaral, 2004).

### 3.1.2 The near infrared window

The near-infrared window (also known as optical window or therapeutic window) defines the range of wavelengths (700-900nm) that can penetrate biological tissues such as skin and blood more efficiently than visible light. "This is mainly due to the fact that within this optical window, the absorbance of the main constituents in the human tissue (i.e., water, oxy-Hb, and deoxy-Hb) is small, allowing the light to penetrate the tissue." (Izzetoglu, Bunce, Izzetoglu, Onaral, & Pourrezaei, 2007, p. 38). Generally, water dominates the photon absorption and attenuation. However, in the optical window water absorption is low enough so that absorbance measurements at a few centimeter deep into biological tissue can be acquired (Madsen, 2013). The 700-900nm range is ideal for optical spectroscopy in tissue because hemoglobin is the main absorber. Within this range, scattering is the dominant light-tissue interaction and propagating light becomes diffused quickly. Scattering increases the mean pathlength travelled by the photon which means the probability of absorption also increases. On the short spectrum of the near-infrared window, hemoglobin is the dominant absorber, as we approach the high-end water absorption becomes increasingly dominant as shown in Figure 2.

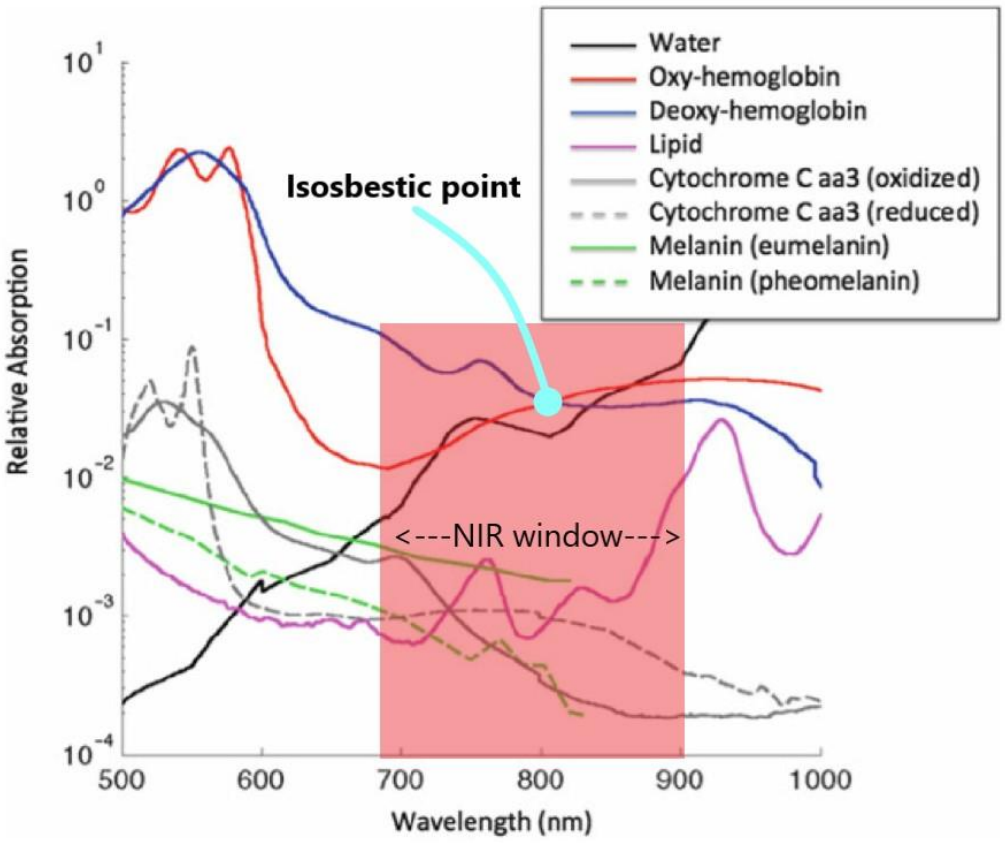


*Figure 2: Absorbing species in the near infrared window. Adapted from (Madsen, 2013)*

### 3.1.3 Optimal wavelength of NIRS application

When choosing the right wavelengths for measuring tissue oxygenation in clinical NIRS applications, the absorption spectra of the main tissue chromophores in the near infrared range must be considered.

> "Among the main absorbers in the tissue, oxy- and deoxy-Hb are strongly linked to tissue oxygenation and metabolism. Fortunately, in the optical window, the absorption spectra of oxy- and deoxy-Hb remain significantly different than each other, allowing spectroscopic separation of these compounds to be possible using only a few sample wavelengths" (Izzetoglu et al., 2007, p. 38).

Wavelengths must be chosen above and below the hemoglobin isosbestic point at around 805nm, where oxy- and deoxyhemoglobin have the same intrinsic absorption coefficient. As shown in Figure 2, HbR is the stronger absorber below the isosbestic point, and $HbO_2$ is stronger above it. It is common to choose a wavelength between 830nm and 900nm as one of the wavelengths because the hemoglobin absorption changes little in this range (Boas, Dale, & Franceschini, 2004). Below the isosbestic point Sato et al. (2004) showed that a wavelength less than 780nm should be used due to lower noise. They also showed that a wavelength around 690nm is more optimal, but that the transparency of the light is lower than in higher wavelengths (Sato, Kiguchi, Kawaguchi, & Maki, 2004).

### 3.1.4 Propagation of light in tissue

In medical applications, the propagation of light in tissue is a complicated matter with an upside and a clear downside. The upside is that biological tissue is fairly transparent to light and allows it to penetrate far inside. This effect can easily be demonstrated by holding a light source to your hand and see the red light glowing through on the other side. The downside is that it is heterogeneous, which means that light will be absorbed differently in relation to the composition of the tissue at each level of depth and scattered in many different directions. This up-/downside is the core of a clear split in optical behavior in tissue. Coherent light is attenuated rapidly as light propagates in tissue, but scattered photons continue to scatter and transport across a large distance. Scattered light is a central feature of light propagation in tissue, with its low tissue absorption and penetration depth, make it a dominant effect in any optical technique (Nolte, 2012). The key question in optical propagation is how much light is scattered and how much is absorbed as light penetrates tissue.

### 3.1.5 Absorption

Absorption is the process where the intensity of a beam of electromagnetic radiation is attenuated in passing through a material by conversion of the energy of the radiation to an equivalent amount of energy appearing within the material. The radiant energy is converted into heat or some other form of molecular energy. The capacity of a material to absorb radiation depends on several factors, mainly the electronic and nuclear constitution of the atoms and molecules of the material, the wavelength of the radiation, the thickness of the absorbing layer, and the variables which determine the state of the medium, of which the most important are the temperature and the concentration of the absorbing agent (McGraw-Hill Concise Encyclopedia of Physics, 2002).
Absorbance is usually given the symbol A, and is the relationship between the initial light intensity ($I_0$) and the intensity that has passed through an absorbing layer (I) given in equation (1):

$$A_l = \log_{10}\left(\frac{I_{l0}}{I_l}\right) \tag{1}$$

Equation (1) will yield a value between 0 and 1, where 0 means that nothing has been absorbed and 1 means that 90% of the light has been absorbed. The absorbance can also be written in the form of Beer-Lamberts law (Clark, 2016):

$$OD = \varepsilon \cdot [\mathrm{X}] \cdot L \tag{2}$$

Where:
OD = optical density (or absorption)
ε = molar extinction coefficient
L = pathlength
[X] = the concentration of the absorbing species

Considering that there is more than one absorbing species in tissue, the above equation can be written in an additive form (Ainslie, 2012):

$$OD = [\varepsilon_1 \cdot [\mathrm{X}]_1 + \varepsilon_2 \cdot [\mathrm{X}]_2 + .. + \varepsilon_n \cdot [\mathrm{X}]_n] \cdot L \tag{3}$$

### 3.1.6 Scattering

Scattering (Figure 3) of electromagnetic waves by any system is related to the heterogeneity of that system. To be considered a scattering event opposed to an absorption followed by an emission the material must interact coherently in a quantum mechanical sense, such that no dephasing intervenes between the incident photon that gets destroyed and the creation of the scattered photon (Kelley, 2012). Bohren and Huffman (1983) describes scattering as following:

> "Matter is composed of discrete electric charges which are electrons and protons. If an obstacle, which could be a single electron, an atom or a molecule, a solid or liquid particle, is illuminated by an electromagnetic wave, electric charges in the obstacle are set into oscillatory motion by the electric field of the incident wave. Accelerated electric charges radiate electromagnetic energy in all directions; it is this secondary radiation that is called the radiation scattered by the obstacle." (Bohren & Huffman, 1983, p. 3)

The transmitted intensity I of a wave decreases exponentially when passing through a scattering media with the thickness x:

$$I_l = I_{l0} \cdot e^{-t_l x_l} \tag{4}$$

Where $I_{l0}$ is the initial intensity, and t is the turbidity (Øgendal, 2017).

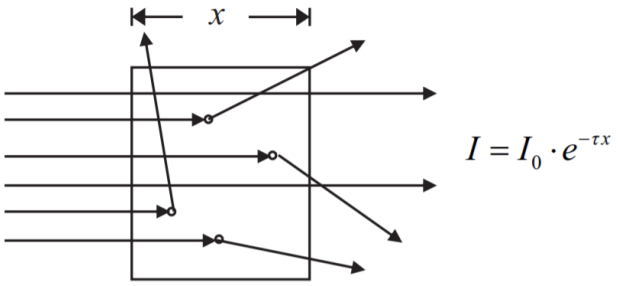


*Figure 3: Decrease of intensity due to scattering (Øgendal, 2017)*

### 3.1.7 Penetration depth

Depth information in NIRS is crucial since the goal is to measure brain activity in specific cortex regions with limited superficial contamination generated by for example the scalp, skull and cerebrospinal fluid. "Depth information is important also for other emerging applications such as cancer screening in thyroid or prostate, or for non-clinical fields, such as internal quality assessment of agricultural produce, non-destructive monitoring of wood materials, or for pharmaceuticals and highly scattering plastics." (Martelli et al., 2016). A comprehensive statistical approach describing the mean maximum penetration depth ($z_{max}$) and mean average penetration depth (z) has been proposed by Martelli et al. and seems to confirm earlier work proposing that: $z \sim \sqrt[2]{d}$ where d is the source-detector separation distance (Weiss et al., 1989), see Figure 4).

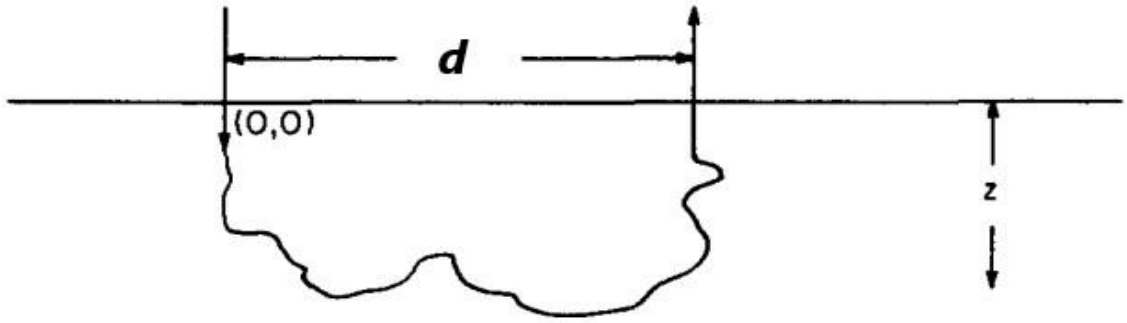


*Figure 4: Typical path travelled by a photon inserted at the point (0,0) (Weiss, Nossal, & Bonner, 1989)*

The figures (Figure 5) below shows the result of a Monte Carlo simulation through a single homogeneous tissue using a 810nm light source, a scattering coefficient of $\mu_s$ = 36.36 $mm^{-1}$ and an absorbing coefficient of $\mu_a$ = 0.09 $mm^{-1}$ (Chatterjee et al., 2015).

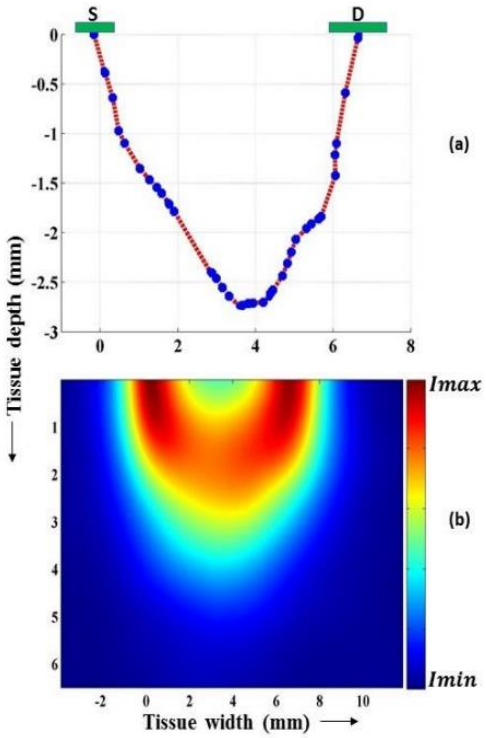


*Figure 5: Path traced for a single photon (a) Distribution of intensity for a photon packet(b) (Chatterjee, Phillips, & Kyriacou, 2015)*

The amount of cerebral contribution of the optical signal is dependent on the penetration depth, and since the depth is less than half than the separation distance between the sensor and detector, short separation covers a great deal of noncerebral tissue. Based on the work of Kohri et al. which shows that at S-D separation of 2, 3 and 4cm, the cerebral tissue contributes to 33%, 55% and 69% to the optical signal, Herold et al. recommends a S-D separation greater than 3 cm for sufficient cerebral contribution to the signal (Herold et al., 2017).

### 3.1.8 Modified Beer-Lambert law

As earlier described, the Beer-Lambert law can be used to calculate the concentration of the absorbing species:

$$[X] = \frac{OD}{\varepsilon \cdot L} \tag{5}$$

Because we want to measure the chromophores in a complex medium, further considerations must be added and is incorporated in the modified Beer-Lambert law (MBLL):

$$OD = \log\left(\frac{I_l}{I_{l0}}\right) = \varepsilon \cdot [X] \cdot d \cdot DPF_\lambda + G \tag{6}$$

Where $DPF_\lambda$ is the differential pathlength scaling factor and G describes the scattering coefficient of the medium together with the geometry of the optodes. G is unknown and therefore an absolute concentration of chromophores cannot be acquired from the above equation. One consequence of this is that only changes in concentration of chromophores can be acquired measured with NIRS (Izzetoglu et al., 2007). If d and $DPF$ is known, quantitative data on the concentration of chromophores can be derived:

$$\Delta OD = \varepsilon \cdot \Delta[X] \cdot d \cdot DPF \tag{7}$$

The concentration changes can now be calculated using different wavelengths for each chromophore of interest by writing a Beer-Lambert law for each and solving the simultaneous equations through matrix inversion as shown here for $HbO_2$ and HbR at time t:

$$\begin{bmatrix}\Delta OD_{\lambda 1}(t)\\ \Delta OD_{\lambda 2}(t)\end{bmatrix} = DPF \cdot d \cdot \begin{bmatrix}\varepsilon_1(\lambda_1) & \varepsilon_2(\lambda_1)\\ \varepsilon_1(\lambda_2) & \varepsilon_2(\lambda_2)\end{bmatrix} \cdot \begin{bmatrix}\Delta HbO_2(t)\\ \Delta HbR(t)\end{bmatrix} \tag{8}$$

Where:
ΔOD is the optical density change.
DPF is the differential pathlength scalar.
d is the distance between the source and detector.
$\varepsilon_n(\lambda_n)$ is the is the molar extinction coefficient at a specific wavelength.
$\Delta HbO_2$ and ΔHbR are the chromophore changes for oxy- and deoxyhemoglobin.

Multiplying the above equation with the inverse of extinction coefficient matrix gives us the concentration change of $HbO_2$ and HbR (Musa, 2015):

$$\begin{bmatrix}\Delta HbO_2(t)\\ \Delta HbR(t)\end{bmatrix} = \frac{\begin{bmatrix}\Delta OD_{\lambda 1}(t)\\ \Delta OD_{\lambda 2}(t)\end{bmatrix} \cdot \begin{bmatrix}\varepsilon_1(\lambda_1) & \varepsilon_2(\lambda_1)\\ \varepsilon_1(\lambda_2) & \varepsilon_2(\lambda_2)\end{bmatrix}^{-1}}{DPF \cdot d} \tag{9}$$

We can now derive the:

1. Oxygenation $\Delta HbO_2$ - ΔHbR
2. Blood volume (tHb) = $\Delta HbO_2$ + ΔHbR

### 3.1.9 Mean optical pathlength

> "Light propagating in the tissue is strongly scattered and the detected light travels considerably farther through the tissue than the distance between the source and detector probes. The quantification of the NIRS signal requires knowledge of the optical path length in the tissue." (Nakamura et al., 2016).

To extract the information on $HbO_2$ and HbR from the measured light intensities using MBLL, the Mean optical pathlength ΔOPL is required. The ΔOPL is given by:

$$\Delta OPL = d \cdot DPF_{\lambda} \tag{10}$$

Where *d* is the S-D separation and $DPF_{\lambda}$ is a wavelength dependent scaling factor that indicates how many times farther than *d* the detected light has travelled.
Duncan et al. has shown that the DPF is age dependent as well as wavelength dependent (Duncan et al., 1996). The following equation (11) is derived by Scholkmann and Wolf takes into account both age and wavelength (Scholkmann & Wolf, 2013):

$$\mathrm{DPF}(\lambda, \mathrm{A}) = \alpha + \beta A^{\gamma} + \delta\lambda^3 + \varepsilon\lambda^2 + \zeta\lambda \tag{11}$$

Where A is the age of the subject,
α = 223.3, β = 0.05624, γ = 0.849, δ = −5.723×10−7δ, ε = 0.001245, and ζ = −0.9025.
α, β, γ, δ, ε and ζ are derived from empirical data.

### 3.1.10 fNIRS

Functional near-infrared spectroscopy (fNIRS) is a non-invasive method of monitoring tissue hemodynamics and oxidative metabolism, specifically in the neuroimaging field aimed at understanding the functioning of the human brain cortex. These measurements are made possible by the fact that biological tissue is mostly transparent to light in the near-infrared range (i.e) 700 – 900 nm (see chapter 3.1.2).

Infrared light propagates through the tissue in a banana-shaped trajectory (Figure 6) and is either scattered by extra- and intracellular boundaries of different layers of the head (skin, skull, cerebrospinal fluid, brain, etc.) or absorbed, mainly by oxy- and deoxy-Hb, though water and other chromophores still affect the intensity of the received light signal. The relationship between the detected light intensity and source intensity is calculated by using the MBLL which explains the absorption and scattering effect in a highly scattering medium (see chapter 3.1.8).

In an effort to try to remove some of the noise introduced to the signal by the extracellular boundaries of the head, some research groups have implemented a short-separation-channel (SSC) and used it to regress the short separation (SS) signal from that of the standard fNIR channel (Brigadoi & Cooper, 2015). This method has shown some hardware challenges, mainly that given the short distance between source and detector, the high intensity of collected light can cause detector saturation.

Figure removed due to Copyright regulations.

*Figure 6: Banana-shaped light path (Bunce, Izzetoglu, Izzetoglu, Onaral, & Pourrezaei, 2006)*

#### 3.1.10.1 fNIRS technologies

There are three different fNIRS technologies, each with their advantages and disadvantages:

- Continuous Wave
- Time domain
- Frequency domain

Below is given a brief review of each of these technologies in the field of fNIRS.

##### 3.1.10.1.1 Continuous Wave

The continuous wave (CW) technology measures light intensity attenuation, using a light source and a photodetector (or similar device). There will be an unknown amount of light loss due to tissue scattering, and the results can thus not be quantified directly, but one can use the modified Beer-Lambert law to linearly relate the changes in attenuation to the extinction coefficient ε (Bakker et al., 2012). CW has some clear advantages, such as size, weight, simplicity and cost, but also a few disadvantages. These include penetration depth and difficulties separating absorption and scattering effects (Bakker et al., 2012), meaning that the level of $HbO_2$ and HbR cannot be determined absolutely (Scholkmann et al., 2014).

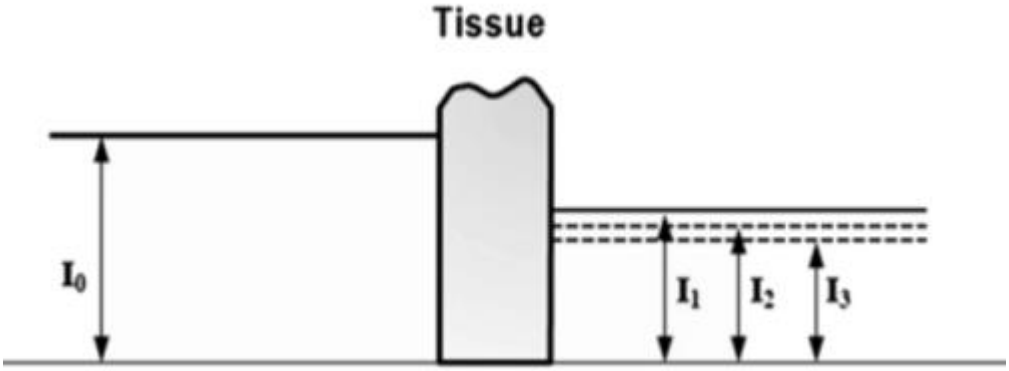


*Figure 7: Concept of CW NIRS (Bakker et al., 2012)*

As seen in Figure 7, light with constant intensity is sent through tissue, and the attenuation is measured.

#### 3.1.10.1.2 Time domain

1996 saw the publication of the first paper on single-channel time domain fNIRS (Torricelli et al., 2014). In time domain (TD) NIRS, a short pulse (just a few picoseconds) is generated and propagates through the tissue. Scattering causes the photons that excite the tissue to have a broad distribution in time. This distribution is called the temporal point spread function (TPSF) (Bakker et al., 2012), or photon distribution of time-of-flight (Torricelli et al., 2014), and can be analyzed in several ways.

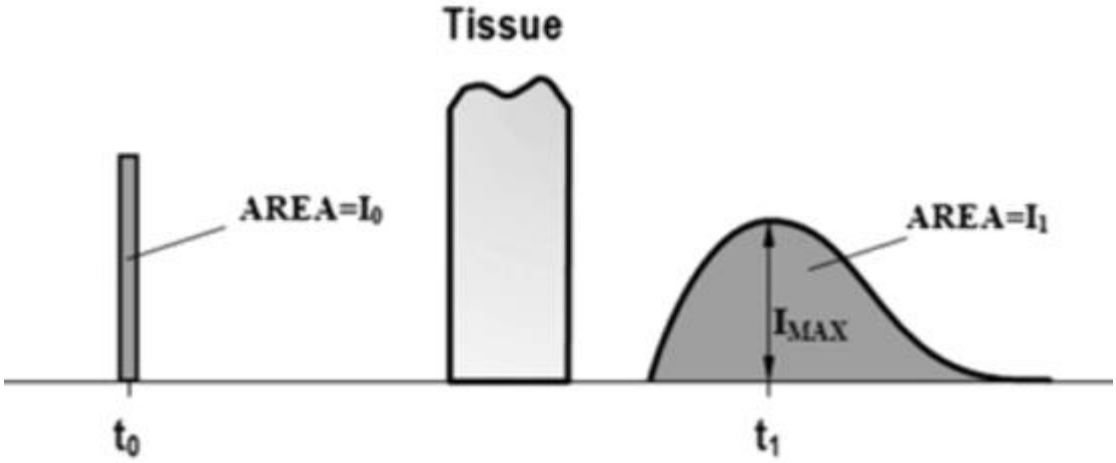


*Figure 8: Concept of TD NIRS (Bakker, Smith, Ainslie, & Smith, 2012)*

As seen in Figure 8 the light pulse is delayed, broadened and attenuated (Torricelli et al., 2014). The delay is simply the time it takes for the light to travel from the source to the detector, the broadening is because of photon scattering and the attenuation is because absorption reduces the probability of detecting a photon.

TD fNIRS is not widely used for commercial purposes today, and it is seen as quite impractical and expensive compared to continuous wave. There are, however, developments being made in the clinical applications of TD fNIRS, especially by European research groups, and technological improvements in fields related to fNIRS, such as electronics, photonics, neuroscience and so forth will contribute to a possibly "flourishing future for TD fNIRS" (Torricelli et al., 2014).

#### 3.1.10.1.3 Frequency domain

Frequency domain (FD) NIRS is a further development of the continuous wave concept, and measures phase shift in addition to light intensity attenuation (Figure 9). This phase shift allows for a more tissue specific quantification of the scattering property, which obviates the need for assuming these values (Davies et al., 2017). According to Davies (2016), there is, however, a need for some assumptions in FD NIRS also. In both cases these assumptions influence how perfusion through the superficial tissue affects the accuracy, and while these effects are known to a large degree for CW NIRS, they are not sufficiently mapped for FD fNIRS (Davies et al., 2017).

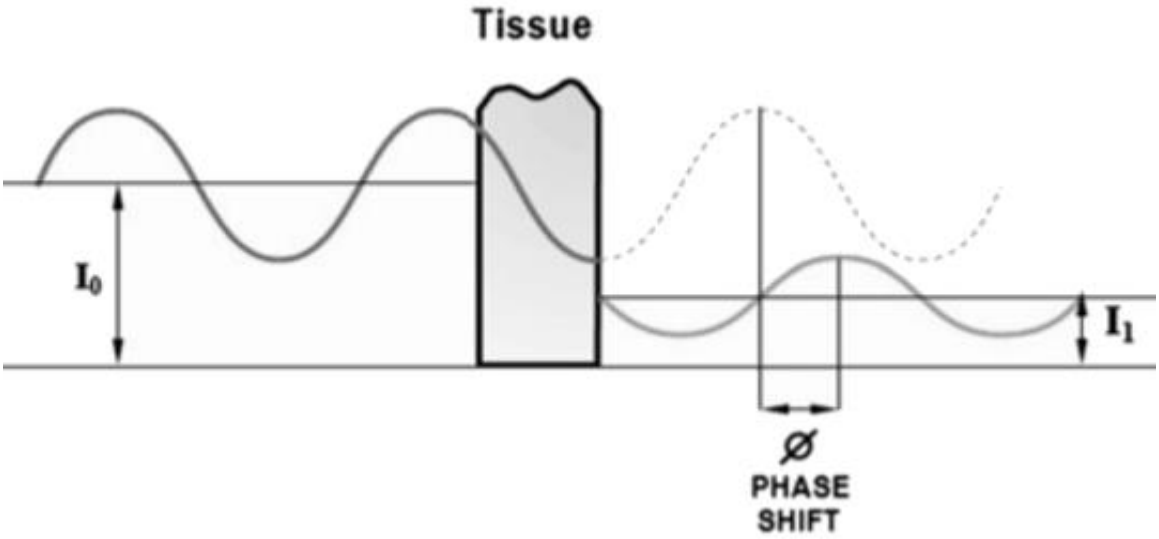


*Figure 9: Concept of FD NIRS (Bakker et al., 2012)*

The theory of photon migration is used to track the photons' movements through tissue, and where CW measures relative changes in different properties, the FD NIRS measure the properties themselves (ISS INC, n.d.).

Neither TD nor FD technologies are widely used for commercial purposes today. Especially TD fNIRS is seen as impractical and expensive compared to continuous wave. There are, however, developments being made in the clinical applications of TD fNIRS, especially by European research groups, and technological improvements in fields related to fNIRS, such as electronics, photonics, neuroscience and so forth will contribute to a possibly "flourishing future for TD fNIRS" (Torricelli et al., 2014).

Even though the CW technology is not the best for measuring absolute values, it is very useful and due to its positive qualities often preferred. In neuroscience it is generally more important

to detect the changes in brain activity, rather than quantifying it in absolute terms (Scholkmann et al., 2014), for which CW fNIRS is sufficient.

#### 3.1.10.2 Artifacts

While fNIRS holds a lot advantages over other methods used for brain assessment, including ease of use and low cost, it is prone to noise and artifacts originating from systemic physiological changes, e.g. muscle activity, heart rate, blood pressure and respiration. These artifacts are particularly problematic during moving (walking, running, jumping, etc.) and talking activities (Vitorio, Stuart, Rochester, Alcock, & Pantall, 2017). Vitorio et. al. reports that there is currently no standard method for identification and removing of these artifacts in moving studies, and propose an important question on whether the mean, maximum, minimum, number of peaks or a combination should be used when the measurement values is being assessed. The mean value is less prone to artifact contamination, but less sensitive to the physiological signal. "Signal processing methods and analysis of fNIRS signals are therefore essential elements in ensuring accurate estimation of the cortical activity from the recorded fNIRS signal." (Vitorio et al., 2017).

#### 3.1.10.3 Short separation channel

The extremities of the human head are highly vascularized and has a mean total thickness of about 13mm in adults, including tissue and skull. Light propagating from a source to a detector must pass through these layers twice, resulting in a lot of attenuation in these superficial layers. This attenuation can be seen as contamination of the fNIRS signal and is one of the biggest challenges in the fNIRS field (Brigadoi & Cooper, 2015).

One way several teams (Gagnon et al., 2011; Koenraadt et al., 2014; Scarpa et al., 2013) has used to try to deal with this problem in CW fNIRS is the multi distance approach (Figure 10). This is simply put: adding another detector closer to the source under the assumption that the photons reaching detector b will have travelled deeper in the tissue than those reaching detector a. The signal from a is then used to filter extracerebral signal from the remaining fNIRS data. The extra detector a is often referred to as a SSC. The optimal distance between the SSC and detector varies across different cortex regions but should generally less than 1cm for measurements on an adults' head (Herold et al., 2017).



*Figure 10: Emitter and detector in short separation configuration*

Brigadoi & Cooper (2015) has reported some challenges in implementing an SSC, one main being detector saturation due to high intensity of collected light. This has earlier been partly solved by employing detector fibers which has a smaller collection diameter. Another has been the implementation of a suitable algorithm to regress the extracerebral signal (Brigadoi & Cooper, 2015).

## 3.2 Anatomy and physiology

### 3.2.1 Skin anatomy

The skin, with a surface area of 1.5 and 2.0 square meters, is the human body's biggest organ. Being the outer layer of the body and interfering with the environment, it plays a significant role when it comes to insulation, sensation and temperature regulation. By providing these functions, the skin is a big part of our immune system.
The skin is all over thicker at men than women and is divided into three layers: the epidermis, the dermis and the hypodermis (Amirlak, 2017). The outermost layer is the epidermis, it is between 0.3 to 1.5 mm thick (Langeland, 2018). This layer is what makes the body waterproof and it consists of approximately 90% keratinocytes. It contains melanocytes which produces melanin and protects the body from UV-rays. The epidermis has no blood vessels and takes all its nutrition from the dermis.
The mid layer is the dermis, it is the thickest part of the skin and gives the skin its elasticity and strength. It contains sweat-glands, hair follicles and a lot of the nerve endings which provide us with the sensation of heat and touch. The dermis provides nutrition and waste-removal for both its own layer and the epidermis.
Hypodermis is the innermost layer and consists of fat and connective tissue. The fat isolates, absorbs shock and works as energy storage (Paulsen & Heir, 2009). Together with the fatty layer, the sweat glands in the hypodermis controls the body temperature. The amount of fatty tissue in this layer is related to the nutrition state and the sex of the person.

### 3.2.2 The human brain and skull

The human brain is commonly divided into two hemispheres; right and left, and into four lobes; the frontal lobe, the parietal lobe, the occipital lobe and the temporal lobe. Each of the lobes and respective hemispheres are associated with distinct functions.

#### 3.2.2.1 The frontal lobe, and the prefrontal cortex

Figure removed due to Copyright regulations.

*Figure 11: The frontal lobe (Dahlitz, 2017)*

The two frontal lobes are placed foremost in the brain (Figure 11), underneath the frontal bone with an average thickness of 6.58 mm at men and 7.48 at women (Li, Ruan, Xie, Wang, & Liu, 2007). They comprise nearly one-third of the brain and is the largest of the lobes. The frontal lobes are, among other things, concerned with processes "involved in motor function, problem solving, spontaneity, memory, language, initiation, judgement, impulse control, and social and sexual behavior" (Center for neuro skills, n.d.). It receives information from the rest of the brain and uses it to carry out decisions and body movements. Damage to this part of the brain can lead to changes in attention, risk analysis, personality and lack of empathy (Cherry, 2018; Richards on the brain, n.d.). The prefrontal cortex is the cerebral cortex which covers the anterior part of the frontal lobe (Dahlitz, 2017), and is divided into multiple functional parts.

- BA10, the anterior prefrontal cortex, has been shown in a number of studies (Allen & Fong, 2008) to be supporting functions like time-based prospective memory, the recognition stage of spatial memory, as well as "high level cognitive processes including risk-taking …". More recent studies also concluded that greater extents of the dorsolateral prefrontal cortex were activated during the time that a test subject was solving matrix reasoning problems.

#### 3.2.2.2 Cerebral circulation

The brain constitutes only 2-3% of the body's total weight but receives typically 15% of cardiac output of the blood and consumes 20% of the oxygen. This is firmly controlled, even if you are asleep or if are focusing on a task, to not increase the intracranial pressure (Harvard University, 2008). However, where in the brain the blood flows do change. If you start to use the occipital lobe, the occipital lobe will get an increased supply of blood and oxygen. The blood in the brain can move around fast and can increase greatly within few seconds if you start using another part of the brain (Cipolla, 2009).

#### 3.2.2.3 Neurovascular coupling

Since fNIRS is an optical neuroimaging method that monitors hemodynamic response to brain activation, it works on the basis that neural activation and vascular response is highly correlated in the way that increased neural activation in one area of the brain, leads to increased blood flow to that same area (León-Carrión & León-Domínguez, 2012). This increase in cerebral blood flow (CBF) during brain activity is dubbed neurovascular coupling. This phenomenon is also what is used in fMRI blood-oxygen-level dependent (BOLD) imaging, which uses hemoglobin as a contrast agent to measure brain activation (Figure 12) (Arthurs & Boniface, 2002). As shown in (Barth & Poser, 2011) a typical (BOLD) hemodynamic response is expected to peak at approximately 5 seconds after initial stimulus.

### 3.2.3 Physiological processes associated with brain neural activity

Figure removed due to Copyright regulations.

*Figure 12: Neural activity leading to hemodynamic response (Arthurs & Boniface, 2002)*

Brain activation is followed by a series of cellular, metabolic and vascular processes and can be summarized as following (Figure 13).

> "Various cellular processes of neurons, such as the restoration of ionic gradients and neurotransmitter recycling, require energy in the form of adenosine triphosphate (ATP). ATP is synthesized first by glycolysis, which is anaerobic and produces a small amount of ATP, and then by oxidative glucose metabolism, which requires oxygen and produces a large amount of ATP. In the brain, about 90% of glucose is metabolized by the latter mechanism, i.e., aerobically. Cerebral metabolism thus depends on a constant supply of both glucose and oxygen. A continuous supply of these two energy substrates is maintained by CBF, which delivers glucose and oxygen to neural tissue through the complex web of blood vessels in the brain's vascular system. Accordingly, during neural activity, increases in oxygen and glucose consumption are followed by an increase in CBF. Whereas the fractional increases in CBF and glucose consumption are similar in magnitude, oxygen consumption increases much *less* than CBF, leading to a net increase in the amount of oxygen present in the blood and tissue." (Pasley & Freeman, 2008).

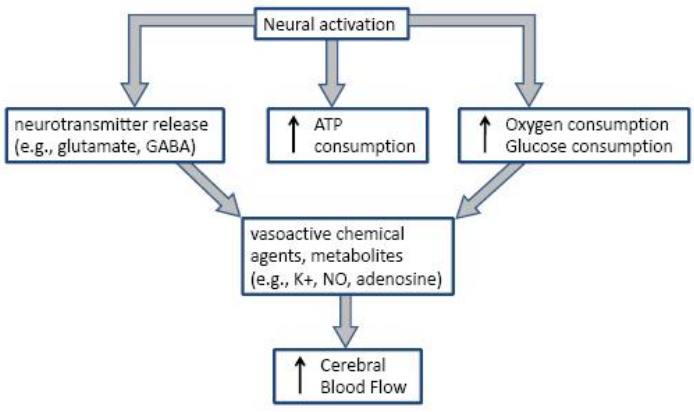


*Figure 13: Summary of physiological changes linking neural and vascular responses. (Pasley & Freeman, 2008)*

## 3.3 Electronics

To measure changes in blood flow and hemodynamic responses in deeper tissues it is important to have a circuit that can deliver precise measurements. It is fundamental to have low noise and off-set, as well as few external disturbances. In this chapter the theory around the chosen solutions will be discussed, as well as the most central and critical devices used in the main circuit and the power supply.

### 3.3.1 Capacitors

Capacitors are passive electronic devices that can store electrical charge and are made up by one or several pairs of conductors separated by an insulator (Figure 14). The capacitance of a capacitor is defined as its ability to store electrical charge. "The capacitance is directly proportional to the surface areas of the plates and is inversely proportional to the separation between the plates. Capacitance also depends on the dielectric constant of the substance separating the plates." (Rouse, 2015).

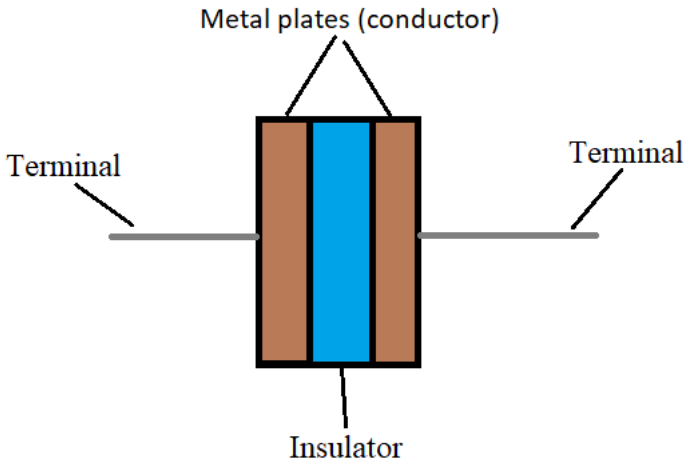


*Figure 14: Capacitor concept drawing*

#### 3.3.1.1 Types of capacitors

- *Electrolytic capacitors* (Figure 15) are polarized capacitors which makes them useless in AC power supplies, but they are widely used in DC power supplies due to their small size and large capacitance. Used mainly to reduce voltage ripples or as decoupling capacitors (ElectronicsTutorials, n.d.-b).

- *Ceramic capacitors* (Figure 15) are non-polarized and are made to give a relative high capacitance in a small body. Mainly used as decoupling capacitors or bypass capacitors due to their large non-linear changes in capacitance against temperature (ElectronicsTutorials, n.d.-b).

*Figure 15: Electrolytic capacitor (left) and ceramic capacitor (right)*

### 3.3.2 Diodes

A diode is a two-lead semiconductor which created by putting a negative- and positive doped semiconductor material together to create a p-n junction (Figure 16). Where these two semiconductors meet there is created an insulating region, which will conduct current in only one direction. When a suitable voltage is applied, electrons can recombine with electron holes within the device. When this happens, the insulating region will disappear and allow current to flow through. Regular diodes are mainly used as rectifiers and are commonly used to convert AC current to DC current in power supplies, as well as to protect components from receiving high voltages (Dahl, 2013).

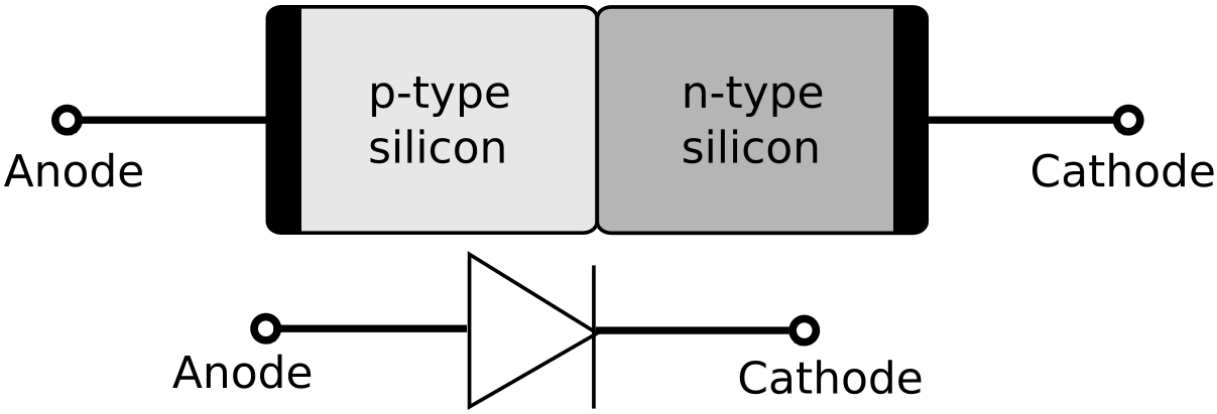


*Figure 16: Diode model*

#### 3.3.2.1 Schottky diodes

A Schottky diode is type of diode that has a very fast switching action and a low forward voltage drop. The voltage drop for a Schottky diode is usually between 0.15 and 0.45 volts, while the forward voltage drop on a regular diode often is as high as 0.6 - 1.7 volts. Because of the low voltage drop of the Schottky diode, there is less energy wasted on heat. These diodes can also be used as rectifier diodes in power supplies (Future Electronics, n.d.).

### 3.3.2.2 Light Emitting Diodes

A light emitting diode (LED) is a diode that emits light when a current pass through it. When a suitable voltage is applied, energy is released in the form of photons. The wavelength of the emitted light is determined by the energy gap (i.e. bandgap) of the diode and the distances between the bandgaps determines the color of the light. The color of light emitted from a LED is not monochromatic, like in a laser diode (LD), but the spectrum is narrow and can functionally be regarded as monochromatic. Since the LED is a p-n junction diode, current flows easily from the p-side (i.e. anode) to the n-side (i.e. cathode), but not easily in the reverse direction. In fact, if the reverse voltage grows large enough to exceed the breakdown voltage, a large current will pass through and the LED may be damaged. A light emitting diode (LED) is favored in many optical neuroimaging systems because of the LED's low power consumption, long life expectancy, high tolerance to humidity, its minimal heat generation, and its low cost.

## 3.3.3 Bipolar Junction Transistor

A BJT is a three-lead semiconductor that is used to amplify or switch electronic signals and power and are one of the most frequently used devices in electrical circuits. The transistor consists of 3 layers of doped semiconductor material, which are either n-doped (negatively charged) or p-doped (positively charged). The three layers can be seen as two diodes (pn-junctions) fused together back-to-back. The BJT is then built up by putting two pn-junctions after each other which makes either a npn- or a pnp-junction (Ingebrigtsen & Nygaard, 2016). The models for the npn-transistor is visualized in Figure 17:

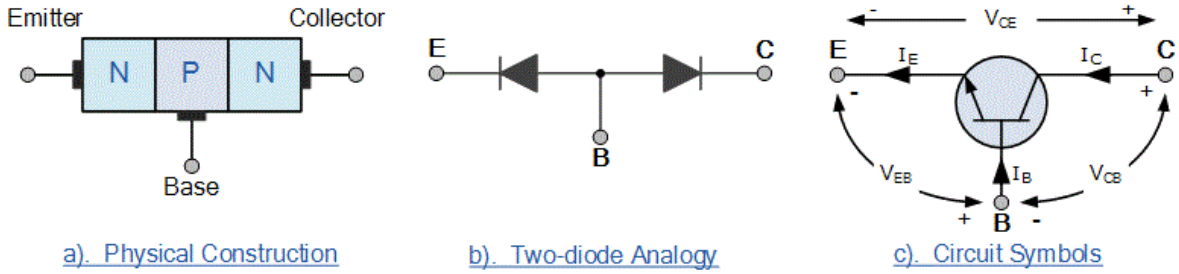


*Figure 17: NPN transistor models (ElectronicsTutorials, n.d.-a)*

As an amplifier a npn-BJT works in a way that allows the current flowing into the base ($I_B$) to control the flow of the current which flows from the collector ($I_C$) to the emitter ($I_E$). The base current is much smaller than the collector and emitter current. At the same time, no current will flow between collector and emitter if there is no current into the base (Ingebrigtsen & Nygaard, 2016). This connection is shown in equation (12):

$$I_E = I_C + I_B \approx I_C \tag{12}$$

The transistors' current gain is given by the β constant which is stated by manufacturer, or it can be measured. The connection between the currents at the inputs of the transistor and the β constant, is given by equation (13):

$$I_C = \beta \cdot I_B \tag{13}$$

### 3.3.4 Voltage regulators

Linear voltage regulators are commonly used to create low power and low-cost applications. The regulator will always provide a steady output voltage even when raising or lowering the input voltage. There are two types of linear regulators, fixed or adjustable (Figure 18). The fixed voltage regulators will always give the voltage output set by the manufacturer, while in the adjustable regulator the output voltage is adjusted using two resistors. There is one downside of these regulators, because it works like a resistor to make a steady output it converts resisted current into heat. Therefore, these regulators are most suited for low power applications where the difference in input voltage and output voltage is low, to minimize the energy wasted to heat (Sattel, n.d.).

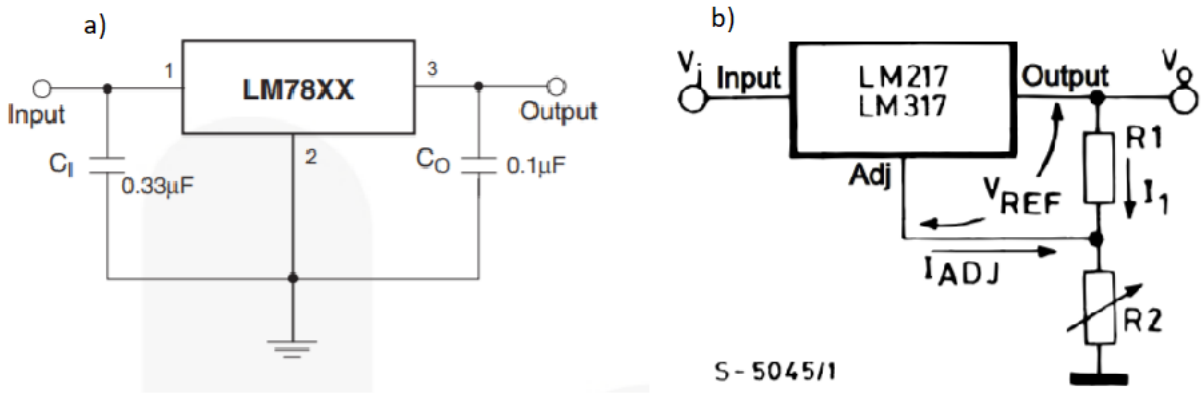


*Figure 18: a) Fixed voltage regulator (Fairchild, 2014) b) adjustable linear voltage regulator (Texas instruments, 2015a).*

### 3.3.5 Voltage follower with transistor current booster

A limitation of many operational amplifiers (opamps) is that they cannot provide a high output current. Typically, an opamp can be expected to maximally source 30 – 40 mA. Though, some opamps can provide higher output current, these are more expensive than general-purpose opamps (Keim, 2016). One way to solve this problem is by buffering the opamp's output current. In Figure 19 we see the schematic of such a circuit.

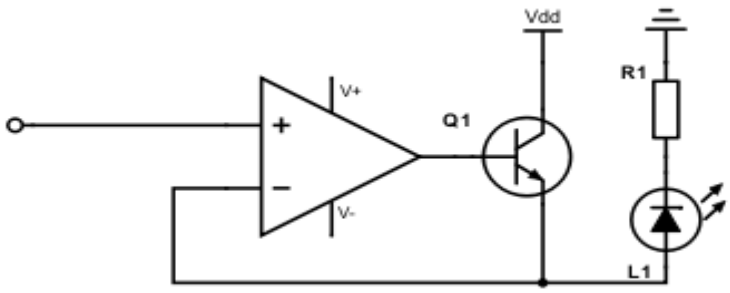


*Figure 19: Voltage follower with transistor current booster*

The purpose of this circuit is to control the voltage of the output, and at the same time provide a higher current than is provided by the output of the opamp (O'Haver, 2008). The output voltage, which is connected to the negative input of the opamp, can be assumed to be equal to the positive input. This is what is called negative feedback, and can be understood by equation (14):

$$V_{out} = A \cdot V_{in} = V_E, \qquad A = 1 \tag{14}$$

As this is a simple voltage follower, the amplification A is equal to 1, and therefore $V_{out} = V_{in}$. For us, this means that the opamp will adjust the voltage at the emitter of the transistor to be equal to that of the input. The output current, at the emitter output of the npn-BJT transistor, is given by equation (15):

$$I_E = I_C + I_B \approx \beta \cdot I_B \tag{15}$$

Where, β (or $h_{FE}$), is the DC current gain which is given by the transistor. This value typically ranges from 50 to as large as 200 for standard npn-BJT transistors.

### 3.3.6 Active positive clipper circuit

In many circuits there are voltage sensitive parts which requires some form of over-voltage protection. One example of a voltage sensitive circuit is the ADC, e.g. the analog inputs of a Genuino Zero have a maximum voltage tolerance of 3.3 V. To achieve such a protection, a clipper circuit can be applied. A clipper circuit can be both negatively and positively biased, depending if it is wanted to protect against negative or positive voltages. In active clipper circuits, a rectifier diode can be used to "clip off" certain parts of a signal. Figure 20 shows an active positive clipper circuit:

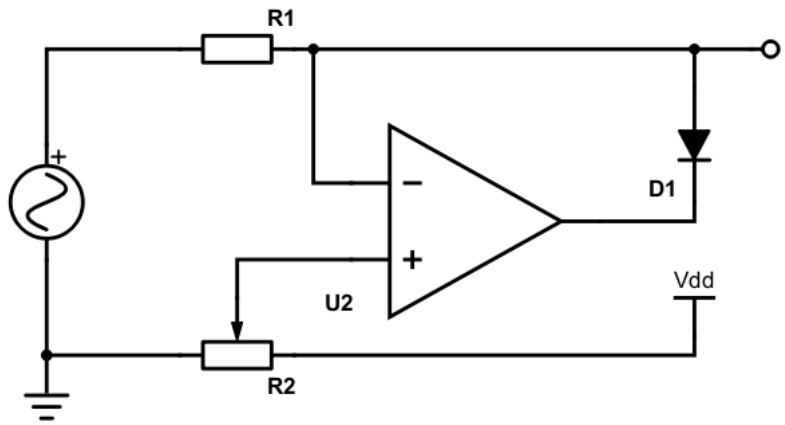


*Figure 20: Active positive clipper circuit*

The voltage level at where the input signal is to be clipped is referenced to the voltage potential at the positive input of the opamp. If $V_-$ (voltage at negative input) becomes a positive voltage above $V_+$ (voltage at positive input), the error voltage will drive the opamp output negative which will turn on the diode. The output will therefore not exceed the voltage which is referenced to $V_+$.

### 3.3.7 Transimpedance Amplifier

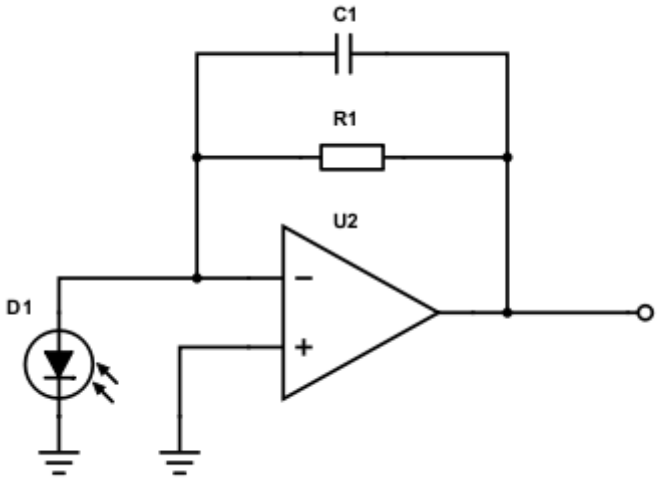


*Figure 21: Transimpedance amplifier*

The transimpedance amplifier (see Figure 21) is a current-to-voltage converter and are widely used together with sensors which have more linear current responses than voltage responses. One such sensor is a photodiode, which is used in this specific circuit. With the TIA a very high gain can easily be ensured with the use of only one resistor, as well as the TIA working as a current-to-voltage converter. The output voltage of the TIA is given by equation (16):

$$-\mathrm{I}_{\mathrm{D}_1} = \frac{R_1}{V_{out}} \tag{16}$$

A typical problem with high gain circuits is noise. There are several types of noise to consider in this circuit (see chapter 3.4), but one other obvious origin of noise is due to amplification of all frequencies. Here is a serious trade-off, because by filtering the noise, the bandwidth is decreased as well as with a narrower bandwidth you get a higher time constant. This is unwanted if the circuit operates at higher frequencies, or if a fast-transient response is vital. As seen in equation (26), the cut-off frequency of a simple RC filter is inversely proportional to the transient response.

#### 3.3.7.1 Parasitic capacitances

"In a physical circuit, parasitic capacitances interact with the feedback resistor to create unwanted poles and zeros in the amplifier's loop-gain response. The most common sources of parasitic input and feedback capacitances are the photodiode capacitance ($C_D$), the op amp's common-mode ($C_{CM}$) and differential input capacitance ($C_{Diff}$), and the circuit-board capacitance ($C_{PCB}$). The feedback resistor, $R_f$ is not ideal and has a parasitic shunt capacitance that may be as large as 0.2pF. In high-speed TIA applications, these parasitic capacitances interact with each other and $R_f$ to create a response that is not ideal" (Cherian, 2016).

This effect means that an LPF is created by these parasitic elements without any actual RC filter purposely being made. The cut-off frequency of this parasitic LPF is given by equation (17):

$$f_{C,-3dB} = \sqrt{\frac{GBP}{2 \cdot \pi \cdot R_f \cdot C_{tot}}} \quad (17)$$

Where:
GBP = the gain-bandwidth product of the opamp
$R_f$ = the resistance of the feedback resistor
$C_{tot}$ = the total parasitic capacitance

#### 3.3.7.2 Oscillation and compensation

When a diode is connected as it is in a TIA, it is known that the circuit it prone to oscillation. This is because the input capacitance of an opamp and its circuitry can cause instability when the opamp is used with a feedback resistor. To solve this instability, it is usually added a feedback capacitor across $R_f$ to stabilize it. To calculate the optimized value of $C_f$, equations (18) and (19) is used, under the given condition (Pease, 2001):

$$i)\ \left(\frac{R_f}{R_{in}} + 1\right) \geq 2 \cdot \sqrt{GBP \cdot R_f \cdot C_s} \rightarrow C_f = \frac{C_s}{2\left(\frac{R_f}{R_{in}} + 1\right)} \quad (18)$$

$$ii)\ \left(\frac{R_f}{R_{in}} + 1\right) < 2 \cdot \sqrt{GBP \cdot R_f \cdot C_s} \rightarrow C_f = \sqrt{\frac{C_s}{GBP \cdot R_f}} \quad (19)$$

Where:
GBP = the gain-bandwidth product of the opamp
$R_f$ = the resistance of the feedback resistor
$R_{in}$ = the shunt resistance of the photodiode
$C_s$ = the photodiode junction capacitance
$C_f$ = the capacitance of the feedback capacitor

### 3.3.8 Sensors

A sensor is a device that takes stimuli from an external parameter (measurand) and responds with an electrical signal that is compatible with an electronic circuit. An electrical signal is something that can be amplified and modified by electronic devices. A sensor's output signal is usually in the form of a voltage, current or charge. The stimuli are the quantity, property or condition that the sensor receives and converts to a signal (Fraden, 2010).

All sensors fall under one of two categories: passive and active. A passive sensor generates its own electrical signal in response to stimulus and does not need any external energy source. Some examples of passive sensors are: piezoelectric sensors, thermocouples and photodiodes. Active sensors need an external power source to operate. The external source is called an excitation signal and the sensor produces the output signal by modifying this excitation signal by response of the stimuli. One example of active sensors is a thermistor, a temperature-sensitive resistor that changes its resistance in relation to temperature (Fraden, 2010).

#### 3.3.8.1 Sensor terminology

Measuring oxy- and deoxyhemoglobin and changes in blood flow can be difficult due to bodily processes and surrounding sources of noise. Below is a description of relevant terms of how reliable a sensor is:

- S*ensitivity* is generally the minimum change in the external parameter that will create a detectable change in the output signal. In some sensors, the sensitivity is defined as the change in input parameter needed to give a standardized output change. In others it is defined as the change in output voltage or current for a given change in output.

- *Selectivity* defines what stimuli the sensor is collecting. This can be problematic as there often are several surrounding stimuli that can affect the sensor (Bochenkov & Sergeev, 2010).

- *Specificity* is defined, in relation to selectivity, how well the sensor is reading the stimuli it is designed to measure and being unaffected by other stimuli.

- *Precision* of a sensor is referred to the reproducibility of a measurement. This means, the degree a sensor can reproduce a value given the same stimulus.

- *Resolution* of a sensor is defined as the smallest incremental change of stimulus, that will be detected at the output signal.

- *Accuracy* of a sensor is the maximum difference between the actual value and the value indicated by the sensor.

#### 3.3.8.2 Photodiodes

A photodiode is a semiconductor coated in silicone that respond to high energy particles or photons. The photodiode absorbs light photons or charged particles to create a flow of current in an external circuit and can be calibrated to give very accurate measurements (Figure 22). Therefore, the silicone photodiode is used in several different devices like spectroscopy and medical imaging instruments. The signal can be measured in both current and voltage, where measuring in current will give a far better result in linearity, offset and bandwidth performance (OSI Optoelectronics, n.d.).

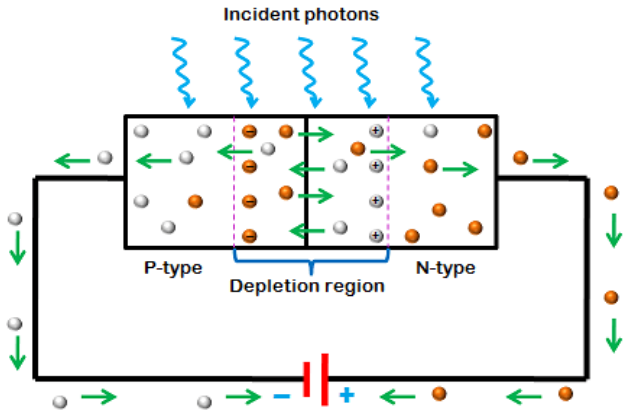


*Figure 22: Photodiode PN junction model (Physics and radio electronics, n.d.)*

A photodiode can be used in two different operation modes, photoconductive and photovoltaic. When using the photoconductive mode, it is applied a reverse bias which will improve the response and the linearity, however it will increase the dark current and noise current, which is making the photodiode more sensitive to temperature as the dark current varies directly with temperature. In photovoltaic mode it is unbiased and is usually preferred when the frequency is low, the application is simple to set up and the response of the photodiode is less sensitive to temperature changes compared to the photoconductive mode, but it will have a slightly slower response time (OSI Optoelectronics, n.d.).

### 3.3.9 Digital-to-Analog Converter

Connecting digital devices with certain sensors and other analog devices requires a system that can convert digital signals, often binary, into a physical measure like a voltage. A DAC is a system that allows the conversion from a digital signal to, in this case, an analog voltage signal output. Below are a description of relevant terms and measures for converters:

- The *full-scale voltage* is given by:

$$\mathrm{FSV} = \mathrm{V_{max}} - V_{min} \tag{20}$$

- The *bit resolution* is given by:

$$Bit\ Resolution = (2^{\mathrm{n}} - 1) \tag{21}$$

- The *resolution*, the smallest measurable voltage, is:

$$Resolution = \frac{Full\ scale\ voltage}{Bit\ resolution} \tag{22}$$

- The *digital value*, related to the output and reference voltage, is given by:

$$\mathrm{Value} = \frac{V_{out}(2^n - 1)}{V_{ref}} \tag{23}$$

### 3.3.10 Analog-to-Digital Converter

To do processing, display and storage of analog signals in computers, there is needed a system that allows for the conversion from an analog voltage signal into a digital signal. Such a system is an ADC. An ADC makes it possible to read an analog voltage signal and quantize it into a digital resolution given by a binary number. Relevant terms and measurements for the ADC is given in equations (20), (21), (22), (23) and (24).

- Relating the input voltage to the ADC to the value it returns digitally, we get (Nate, n.d.):

$$\frac{ADC\ resolution}{System\ voltage} = \frac{ADC\ reading}{Measured\ voltage} \tag{24}$$

### 3.3.11 RC filter

An RC filter is an electric circuit consisting simply of resistors and capacitors, used to block out unwanted frequencies while allowing others to pass. Depending on which frequencies that are unwanted, one could apply either an LFP, HPF or BPF. An LPF filters out frequencies above a given cut-off frequency, an HPF the frequencies below, and a BPF blocks out the frequencies outside a given range of frequencies and can in its simplest form be a combination of an LPF and HPF. The cut-off frequency is given in equation (25):

$$f_c = \frac{1}{2 \cdot \pi \cdot R \cdot C} \tag{25}$$

Another value to take into consideration when designing RC filters is the time constant, τ. The time constant is also called the transient response, which is the time the capacitor needs to charge up to 63.2% of the applied voltage. Because of this transient response, we will be able to see a load-up and load-out curve which will be proportional to the size of the resistor times the capacitor. The time constant for a RC filter is given in equation (26):

$$\tau = R \cdot C = \frac{1}{2 \cdot \pi \cdot f_c} \tag{26}$$

Where $f_c$ is the cut-off frequency of the RC filter.

In high-speed applications it is vital that this constant is as low as possible, so that too much of the actual signal will not be cut out by this response.

### 3.3.12 Microcontroller unit

A microcontroller is a computer that is in a single IC. The chip usually includes CPUs, memory, programmable I/O peripherals and more, and is widely used in a wide array of products and devices that needs any degree of automation control.

### 3.3.13 Integrated Development Environment

IDE is a software application that is used to write, debug, compile and upload computer code from a PC to a physical board, in this case an MCU.

## 3.4 Noise

### 3.4.1 Johnson noise

Johnson noise is often referred to as thermal noise and is generated by thermal fluctuations in conducting materials. It is a result of random motion of electrons in a resisting material, and occurs when electrons collide with each other or the atoms in the material. Each motion of an electron between collision represents a small current, and although the sum of all these currents over a long-time period is zero, their random fluctuation over a small interval constitutes the thermal noise. One way to reduce the thermal noise of a system is to cool the resisting materials, and thereby reducing the random motion of the matter. Johnson noise is given by equation (27):

$$e_n = \sqrt{4 \cdot k \cdot T \cdot R} \quad (27)$$

Where:
$e_n$ = is the Johnson noise voltage
k = Boltzman constant
T = the absolute temperature in kelvin
R = is the resistance given in ohms

For a given system bandwidth the Johnson noise is given as equation (28):

$$e_n = \sqrt{4 \cdot k \cdot T \cdot B \cdot R} \quad (28)$$

Where B is the bandwidth in hertz over which the noise is measured (Johnson, 2003).

### 3.4.2 Shot noise

Shot noise occur due to the quantum nature of electrons and photons and is the uncertainty in determining the magnitude of a current. It appears to only originate in systems where a "barrier" is present, like in a photodiode. Photons being quantized and discrete, the same amounts of photons do not hit the photodiode at the same time, resulting in random fluctuations in the photon-electron conversion. If a large amount of measurements is made of an apparently constant current, the resulting plotting should be evenly distributed around the apparent value, as seen in Figure 23.

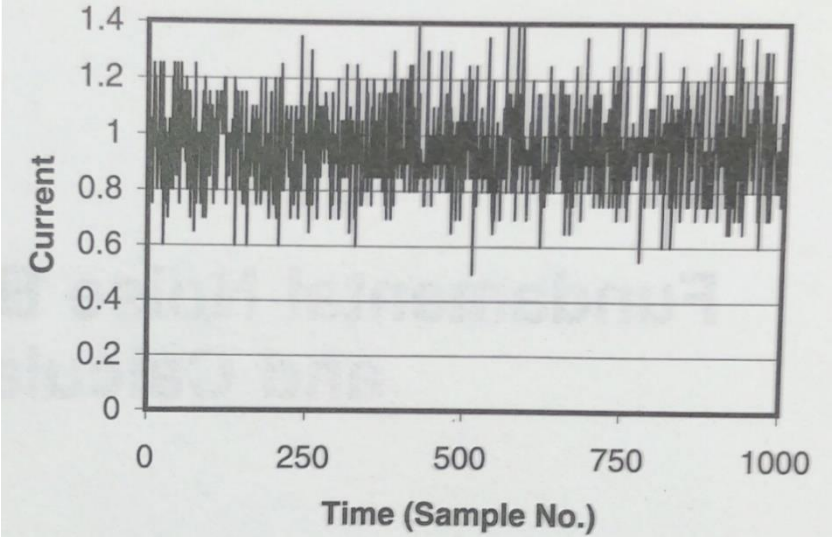


*Figure 23: Shot noise (Johnson, 2003)*

The current noise power spectral density ($i^2_n$) of a constant photocurrent is given by the Schottky equation (29):

$$i_n^2 = 2 \cdot e \cdot I_p \cdot B \quad (29)$$

Where e is the electron charge ($1.602 \cdot 10^{-19} C$) and B is the bandwidth in hertz (Johnson, 2003).

# 4 System design

This chapter describes the individual parts of the instrument (Figure 24), what choices were made and how the instrument was but together. But first the protocols that will be used to validate the system will be introduced.

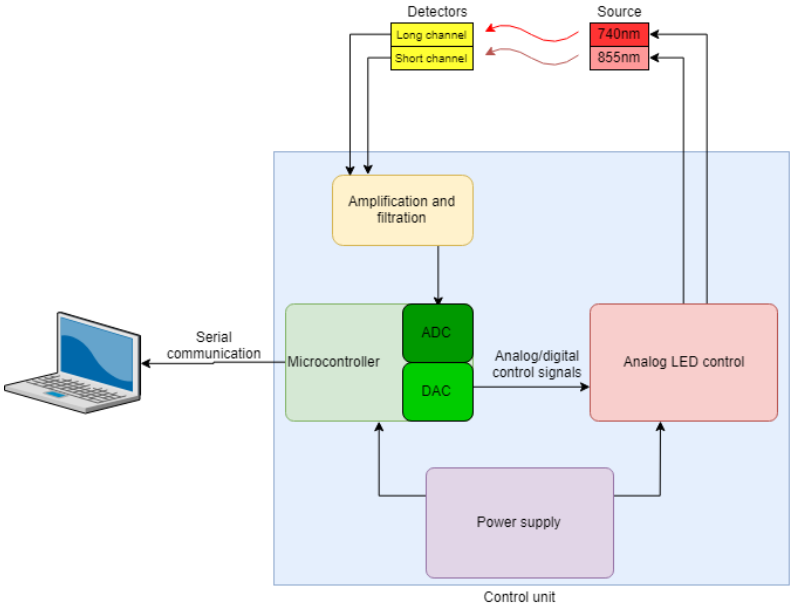


*Figure 24: Graphical overview of the instrument*

## 4.1 Experiment test protocols

Prior to designing the protocols, a number of pilot studies were conducted to search for trends, as well as conversations with our project advisor and a psychologist specializing in neuroscience and behavioral science. Our pilot study also unraveled several error sources which we had to consider when designing the protocol tests.

Protocol 1 generated clear trends in terms of absorbance, meaning we saw significant changes in signal. The observation of this clear trend (during the pilot study) due to reduced blood flow in the arm, made this test become basis for further testing.

Protocol 2 was mainly designed through feedback and comments made in conversations with out project advisor and a psychologist who has made familiar protocols for fNIRS tests earlier. The pilot study for this test protocol contained different cognitive tests than those we were later advised to use and was therefore changed. As well, the pilot study showed us that verbal tests were a poor choice because it added artifacts to the readings. Protocol 2 therefore was designed to be non-verbal.

### 4.1.1 Test protocol 1: Cuff

This protocol aims at examining how the NIR signals are changed and affected by a forced change in blood flow, and to observe the correlation between change of blood flow and change in number of photons reaching the photo sensors.

*Figure 25: Demonstration of probe placement for test protocol 1*

Prior to the test, the probe and cuff are placed on the test subjects' arm. The test subject shall be seated straight up in a chair with both arms placed at an arm rest with the elbow in a 90-degree angle and sitting still during the whole test sequence. The probe is placed at the middle of the anterior antebrachium (forearm) relative to the length of test subject's antebrachium, see Figure 25). The probe should not be fastened too hard as this alone will affect the blood flow of the arm. The cuff is placed around the brachial region (upper arm), comfortably and not too tight. The test subject shall not experience pressure from the cuff until the active part of the test.

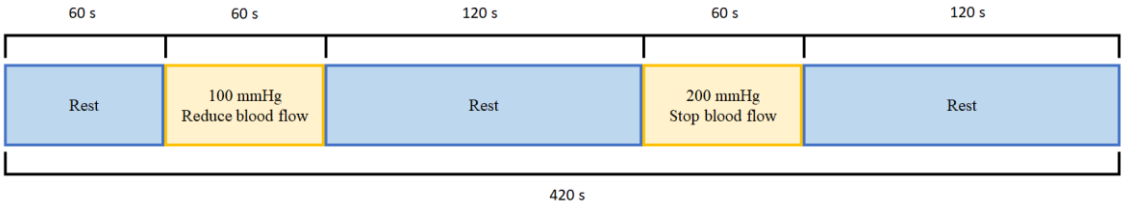


*Figure 26: Timeline test protocol 1*

The total estimated time of the test is 420 s, with rest periods of 120 s after each stimuli to allow circulation to return to baseline (Figure 26); LT of PORH (Baric, Stupin, Bari, & Drenjancevic, 2013).

### 4.1.2 Test protocol 2: Prefrontal Cortex

This protocol aims at examining how the NIR signals are changed and affected by the changes in cerebral circulation during a non-verbal test, which stimulates the prefrontal cortex, and to observe the correlation between change of blood flow and change in number of photons reaching the photo sensors.

*Figure 27: Demonstration of probe placement for test protocol 2*

To begin the test, the probe is to be placed at the test subjects' sinciput (forehead), see Figure 27). The test subject shall be seated straight up in a chair with both arms placed at an arm rest with the elbow in a 90-degree angle and sitting still during the whole test sequence. It is especially vital not to wrinkle the forehead during this test, and not to talk, unless it is noted in the protocol specifically. The probe is placed horizontally at the upper middle of the sinciput, along the transversal axis. The probe should not be fastened too hard, but it must be made sure that both sensors and all diodes are in contact with the skin at the sinciput. The test will begin with a period of rest to settle the baseline for the measurements, as well as letting the test subject find comfort in the test position.

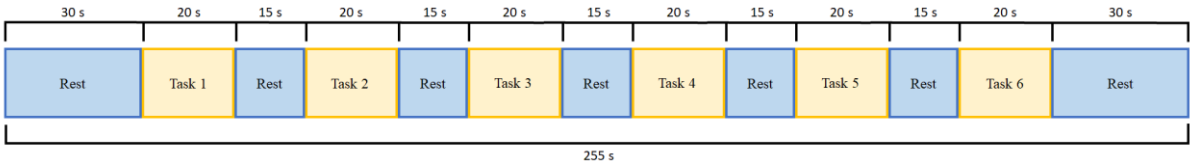


*Figure 28: Timeline test protocol 2*

After a period of rest to set a baseline for the measurement, there will be given six cognitive ability tests with a period of rest in between. The periods of rest will consist of the test subject sitting still and gazing at a small cross placed in the middle of the screen for 15 s. The total estimated time of the test is 255 s (Figure 27).

### 4.1.3 Experiment surroundings

For each test conducted, two persons were present in the room together with the test subject. One controlled the computer and timing, the other controlled the answers of the test subject. The same room was used for all tests conducted. The room had ambient light, but the ceiling lights were turned off and blinds covered the windows letting only a minimum of sun light through. Ambient temperature was measured to be 23 ± 2 degrees Celsius. To avoid temperature drift of the sensor, the sensor was worn by the test subject of a minimum of 3 minutes before

any test protocols were started. To ensure the correct placement of the sensors and that each test subject would have similar test conditions, the placement of the sensors and the chair was marked.

## 4.2 Electrical circuitry

### 4.2.1 Microcontroller

The Genuino Zero (Figure 29) has one built-in 10-bit DAC that easily can be used for signal generation, as well as 6 12-bit ADC channels that can be used for signal acquisition. To create the signal form there were used MATLAB scripts to generate arrays containing the values corresponding to the desired signal form. Some features and advantages of the Genuino Zero (Arduino, n.d.-a):

- 1 10-bit DAC output
- 6 12-bit ADC inputs
- Clock speed of 48 MHz
- Operating voltage 3.3 V
- Recommended input voltage 7-12 VDC or USB 5 V
- DC current output 7 mA
- USB input for power supply and serial communication


*Figure 29: Genuino Zero (Arduino, n.d.-a)*

The Genuino Zero was chosen for the project as it has an easy-to-handle interface, together with a DAC, ADC and the possibility to communicate over USB with a PC. This makes the process of generating and reading the signals easy, as well as giving the opportunity to send the sensor values serially to a PC for processing and plotting with a USB connection.

#### 4.2.1.1 Micro USB connection

After the Genuino Zero has collected the sensor data and converted it into digital values through the ADC, the data is sent to a PC via USB connection. The micro USB cable is connected to the *USB programming port* of the Genuino Zero which is connected to the Atmel EDBG. The Atmel EDBG behaves like a USB-to-serial converter which in order is connected to the first

serial interface (UART) of the SAMD21 microcontroller (SM, 2018). Features and things to consider when using the USB connection with an Arduino/Genuino board:

- When using the Serial function, pins 0 and 1 cannot be used as I/O (Arduino, 2018).
- The Genuino Zero can be supplied with 5 V from the USB during serial communication
- The ADC will return a value between 0 and 4096, when set to 12-bit resolution

### 4.2.2 ADC and DAC

The microcontroller unit has an internal DAC and ADCs, which can provide or receive a maximum of 3.3 V. The resolution of the Genuino zero ADC and DAC is given in equations (30) and (31), assuming 12- and 8-bit resolution respectively.

$$\frac{Full\ scale\ voltage_{ADC}}{Bit\ resolution_{ADC}} = \frac{3.3\ V}{2^{12}\ bits} = 0.805664\ \text{mV/bit} \tag{30}$$

$$\frac{Full\ scale\ voltage_{DAC}}{Bit\ resolution_{DAC}} = \frac{3.3\ V}{2^{8}\ bits} = 12.890625\ \text{mV/bit} \tag{31}$$

### 4.2.3 Analog switch and amplification

To switch the source signal to several different LEDs, a 4066 Quad Bilateral Switch IC was used. The control inputs of the 4066, which controls the switches, are toggled by three of the digital outputs of the Genuino Zero. Three switches are used to switch between each of the LEDs. The pin configuration of the 4066 is shown in Figure 30.

Some features of the 4066 are as follows (GS, n.d.):

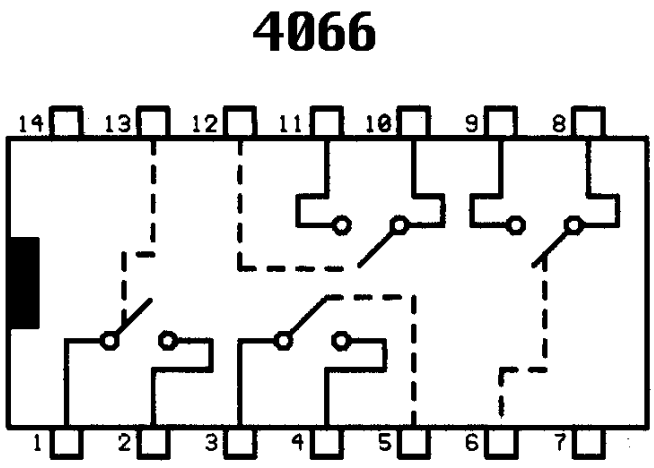


*Figure 30: Pin configuration of 4066 analog CMOS switch (Knopp, 1997)*

- Propagation speed: $t_r = t_f = 20$ ns
- Single supply voltage: 3 - 18 V

### 4.2.4 Light emission source

When we were considering a light source for our system, there were mainly two kinds of emitters to consider, LEDs and laser diodes (LD). Our choice fell on using LEDs, mainly due to the low cost, wide range of available wavelengths, and the fact that unlike LDs it doesn't need complex and bigger drive circuits. Table 2 shows a comparison of LED and LD used for fNIRS.

*Table 2: Comparison of LED and LD for use in fNIRS*

| | | |
|---|---|---|
| **LD** | *Pro* | • Coherent and almost monochromatic light emission.<br>• Allows higher power output during pulsatile operation |
| | *Con* | • Limited availability in different wavelengths.<br>• Higher safety demands<br>• Requires bigger control circuits<br>• Expensive<br>• Generates a lot of heat and often requires optical fibers to carry light to tissue. |
| **LED** | *Pro* | • Available with a higher range of different wavelengths<br>• Minimal power consumption<br>• Minimal heat dissipation problems<br>• Usually cheaper than laser diodes<br>• Available in packages containing several individual and controllable wavelengths. |
| | *Con* | • Nonmonochromatic light emission, spectrum bandwidth typ. 20-50nm. |

We chose a multiwavelength LED (L735/805/850-40C32, manufactured by Ushio, (Figure 31 A)) which contains 735 nm, 805 nm and 850 nm in one packet. These wavelengths were chosen regarding the work reviewed in chapter 3.2.6, and because of verbal recommendations from our project advisor. The specific LEDs were chosen because they were available in multiwavelength packets, they have a narrow spectral bandwidth (Figure 31 B) and a high radiant intensity (Figure 31 C).

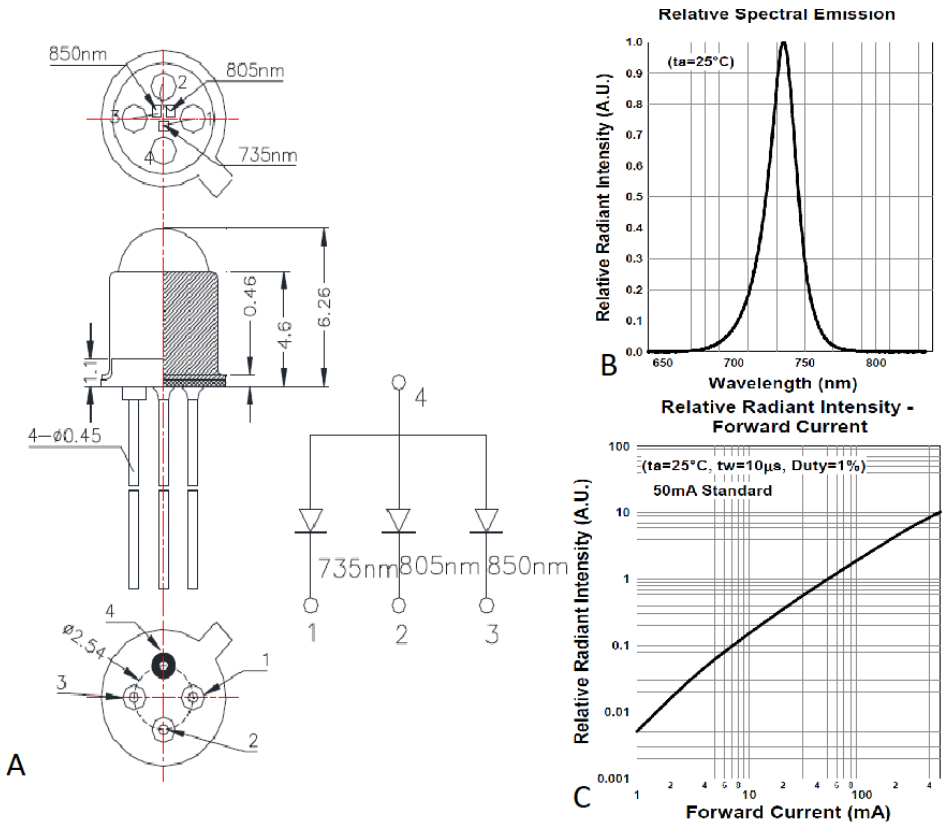


*Figure 31: A) Ushio L735/805/850-40C32 B) Spectral bandwidth of L735/805/850-40C32 C) Radiant intensities of L735/805/850-40C32 (Ushio, 2017)*

Unfortunately, the LEDs did not arrive before the project was due, so we ended up using two readily available surface mounted LEDs manufactured by OSA optolight (Figure 32 A), one 740nm (OIS-330 740) and one 855nm (OIS-330 IT855), which fitted our design well. They also have a narrow spectral bandwidth (Figure 32 B), though not as sharp as the Ushio LEDs. Table 3 shows the most important characteristics of the LEDs.

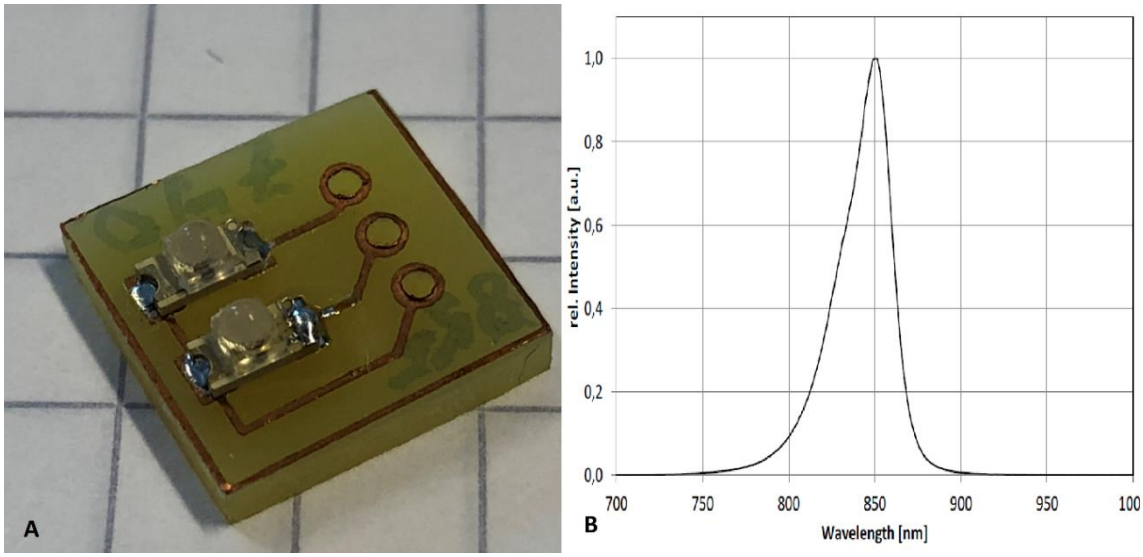


*Figure 32: A) 740nm (upper) 855nm (lower) B) Spectral bandwidth of the OIS LEDs (OSA opto light, 2012)*

*Table 3: OIS-330 740 and OIS-330 IT855 characteristics (OSA opto light, 2012)*

| *Characteristics* | 740nm | 855nm |
|---|---|---|
| *Typical total radiated power* | No data | 30 mW ($I_f$ = 50 mA) |
| *Max forward current ($I_f$)* | 30 mA | 50 mA |
| *Max pulsated forward current (tp ≤ 100 µs, τ = 1:10)* | 100 mA | 100 mA |
| *Forward voltage* | 1.7 V | 1.55 V |
| *Half Width Δλ* | 30 nm ($I_f$ = 30 mA) | 30 nm ($I_f$ = 50 mA) |

### 4.2.5 LED's control circuit

To control the output to the LEDs, it was added a non-inverting opamp to amplify the signal originating from the Genuino Zero as well as a current booster circuit (see chapter 3.3.5) to supply sufficient current. The non-inverting opamp was added to boost up the signal originating from the Genuino Zero to supply the LEDs with sufficient voltage. This signal originally has a maximum value of 3.3 V, and is amplified to 5.1 V. The calculation of the amplification is given in equation (32).

$$\mathrm{V_{out}} = \mathrm{A} \cdot \mathrm{V_{in}} = \left(1 + \frac{R_f}{R_1}\right) \cdot \mathrm{V_{in}} \implies 5.1\,V = \left(1 + \frac{18\,k\Omega}{33\,k\Omega}\right) \cdot 3.3\,\mathrm{V} \qquad (32)$$

When the amplified signal comes from the non-inverting opamp, it passes through the current booster circuit. The opamps used (TL072 and TL074) have a maximum output current of 25mA, which is not enough to supply the chosen LEDs. In this circuit the opamp will only have to supply the base current of the transistor while the current at the collector of the transistor, which is much higher, sources the LEDs. The negative feedback loop ensures that the output voltage of the opamps will be equal to the input voltage, and continuously will regulate itself to it. With this circuit, the LEDs will be sufficiently supplied with current from the emitter of the transistor as well as being fed the same voltage that is at the positive input of the opamp.

### 4.2.6 Signal

Most CW based fNIRS systems are today based on continuous amplitude signals. It was however proposed, that it would be interesting to experiment with the signal wave, especially until the point where the short-channel photodiode reaches saturation. One idea was to try a chirp signal; a signal which increases in frequency. We, on the other hand, focused the project into amplitude modulation signals. The signals were designed for each LED, so they would begin each wave at the specific LED's forward voltage and continue in steps up to ~5 volts.

### 4.2.7 Photodetector and transimpedance amplifier

When considering what type of photodetector there was mainly three distinct types to consider:

- PMT – Photomultiplier tubes (Lühmann, 2014) (Abramowitz & Davidson, n.d.).
- APD – Avalanche Photodiode (Spring, Long, & Davidson, n.d.).
- SPD – Silicon PIN Photodiodes (Lühmann, 2014) (Hamatatsu, n.d.).

There are other photodiode types available, but silicon semiconductors are favorable due to higher sensitivity and better noise characteristics in the NIR spectrum compared to others (Lühmann, 2014). To make a contemplated decision of which photodetector to choose we created a table (Table 4) to compare the three distinct types listed above.

*Table 4: Comparison Photodetectors*

| | | |
|---|---|---|
| **PMT** | *Pro* | • Can sense very weak light (Gold standard sensitivity)<br>• Built in amplification (gain over 100 million)<br>• Low dark current<br>• Can detect extremely fast events |
| | *Con* | • Require high voltage supply (500 - 2000 V)<br>• Sensitive to a wide specter of wavelengths (110 - 1100 nm)<br>• Large in size<br>• Require cooling<br>• Sensitive to magnetic fields |
| **APD** | *Pro* | • Built in amplification (gain 500 - 100)<br>• Compact<br>• Immune to magnetic fields<br>• Require low current<br>• Can sense very weak light (Higher than PDs) |
| | *Con* | • Substantial dark current<br>• Require high voltage supply<br>• Require cooling (high bias voltage) |
| **SPD** | *Pro* | • Small in size, and cheap<br>• Low voltage supply<br>• Low dark current<br>• No cooling necessary<br>• High speed response |
| | *Con* | • No built-in amplification<br>• Lower sensitivities than PMTs and APDs |

Other work groups making similar instruments chose the SPD because of several factors, including:

- the SPDs can be applied directly to the surface, unlike PMTs and APDs, which "traditionally require optical conduction with optical fibers" (Lühmann, 2014)
- High dynamic range (Fatmehsari, 2015) (Lühmann, 2014)
- Stabilized supply voltages (Fatmehsari, 2015) (Lühmann, 2014)

Also, regarding the advantages and disadvantages in Table 4 the choice fell on the silicone photodiode because of its small size, low voltage supply and that it does not need cooling.

The photodiode used for this project, the OPT101 (see Figure 33), is a monolithic photodiode with an on-chip TIA. The TIA circuit within the OPT101 is also optimized to eliminate problems commonly encountered in discrete designs, such as leakage currents, noise pick-up, and gain peaking as a result of stray capacitance (Texas Instruments, 2015b). Some other desired features of the OPT101 are as follows (Texas Instruments, 2015b):

- Designed for single or dual power supply operation, 2.7 to 36 V
- Has a high responsivity of 0.45 A/W at 650 nm
- Output voltage responsivity of approximately 0.45V/µW at 650 nm
- Rise time (10% - 90%), $t_r$, of 25 µs
- Has a wide bandwidth of 14 kHz
- Is recommended for medical instrumentation

As seen in the spectral intensity curve in Figure 33 c), the responsivity of the OPT101 is at least ~85% to its peak value for all our chosen wavelengths (740 nm, 855 nm).

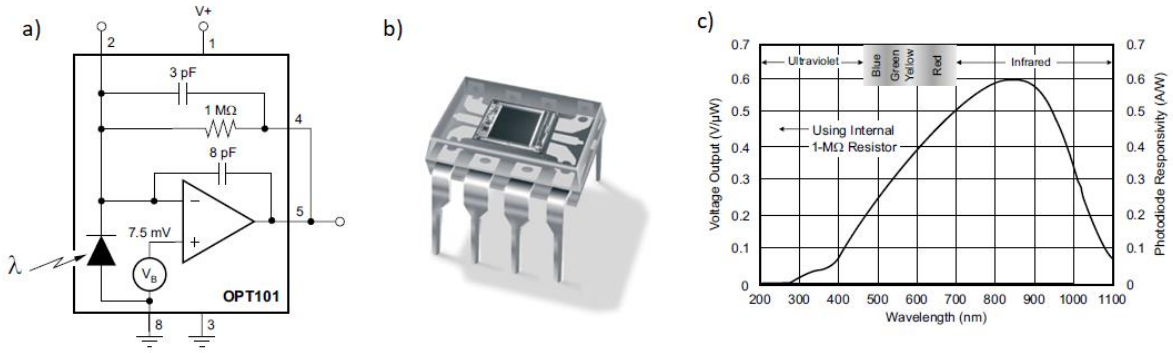


*Figure 33: a) OPT101 block diagram. b) OPT101 detector. c) Spectral responsivity curve of OPT101 (Texas Instruments, 2015b)*

#### 4.2.7.1 Additional filtering and amplification

The OPT101 is compensated and optimized for its intended use. It is difficult to increase the amplification of the OPT101's TIA without affecting its response to an undesirable degree. For long channel it was necessary to increase amplification in order to make use of the ADCs' dynamic range. To avoid affecting the response of the OPT101 we decided to do all additional amplification and filtering in cascade with the OPT101 instead of adding elements to the IC itself, like additional feedback resistors or an LPF.
For both channels the internal 1 MΩ resistor was used as main source of amplification, while for the long channel we added another non-inverting amplifier and a passive RC LPF. The LPF was added due to higher noise of long channel than short channel, because of the additional amplification. A potentiometer was added to manipulate the amplification over the non-inverting amplifier, as shown in the equations (33) and (34).

$$f_c = \frac{1}{2 \cdot \pi \cdot R \cdot C} = \frac{1}{2 \cdot \pi \cdot 1.5\ k\Omega \cdot 0.1\ \mu F} \approx 1061\ \text{Hz} \qquad (33)$$

$$A = 1 + \frac{R_f}{R_1}$$

$$\text{where,} \quad \frac{0\ \Omega}{1\ k\Omega} < \frac{R_f}{R_1} < \frac{500\ k\Omega}{1\ k\Omega} \tag{34}$$

### 4.2.8 Noise

Noise considerations are important for any electrical circuit, and especially in high-frequency and switching circuits. Listed are some considerations and improvements that were made:

- *Bypass capacitors*: Recommendations from datasheets have been followed regarding bypass capacitors for all ICs including placement within close proximity of the IC (Texas Instruments, 2015b) (GS, n.d.) (Texas Instruments, 2017).
- The *type of cables* used can be central in generation of noise in a circuit. Artifact noise occurring because of movements of the cables between the circuit and the probes was a major problem during the test phase. We tested different shielded cables for this purpose, as well considering the movability of the test subject. For the purpose, we did a test of three easily accessible cables, namely the Profibus 3079A 1PR22, R&M Cat 5E UTP and NEK MT-2/B (a shielded twisted pair cable (2 x 0.14 $mm^2$), out of production). Even though the NEK MT-2/B was not the top choice regarding noise, it was considerably better than the alternatives when considering movability and weight. We therefore chose the NEK MT-2/B (Figure 34), and for the purpose of testing the circuit decided to minimalize the movability of the test subject.

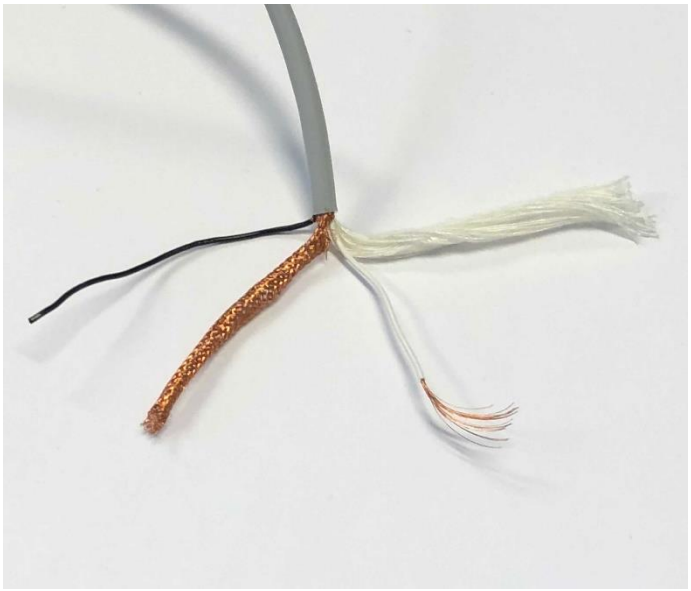

*Figure 34: NEK MT-2/B*

### 4.2.9 Power Supply

For the power supply we needed both +9V and -9V to power the opamps in the main circuit as well as a +5V output for the rest. To get a negative voltage we used a voltage divider and made sure we had a steady voltage at the outputs by using three 3-terminal fixed regulators, one for

+9V (7809), one for -9V (7909) and one for +5V (7809). Because we wanted a way to know when the power supply was turned on/off we added a LED indicator which will indicate if the power supply is active or not. To find the resistor needed for the LEDs we looked at the forward current in the datasheet (Avago, 2015) which was 25mA and used Ohm's law (35) and (36).

$$V = R \cdot I \tag{35}$$

$$R_5 = \frac{V_{tot} - V_F}{I_F} = \frac{9V - 2{,}7V}{25mA} = 252\ \Omega \tag{36}$$

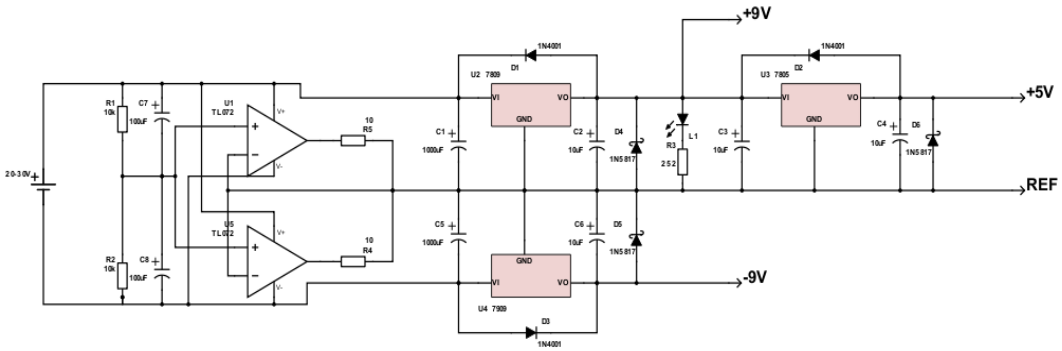


*Figure 35: Power supply schematic*

### 4.2.9.1 Voltage divider

To create a positive and negative voltage we used a simple voltage divider (Figure 36) with the associated equation 37 followed by two noninverting opamps (TL072) circuit with unity gain (also called a buffer) to make sure the divider is not affected by the rest of the circuit and creates an uneven output (Horowitz & Hill, 2015). When using the opamp we encountered a voltage drop on the output, this was because the opamp could not provide enough current, this was solved by adding a second opamp to provide enough current to avoid the voltage drop.

$$\frac{Vout}{Vin} = \frac{R_2}{R_1 + R_2} \tag{37}$$

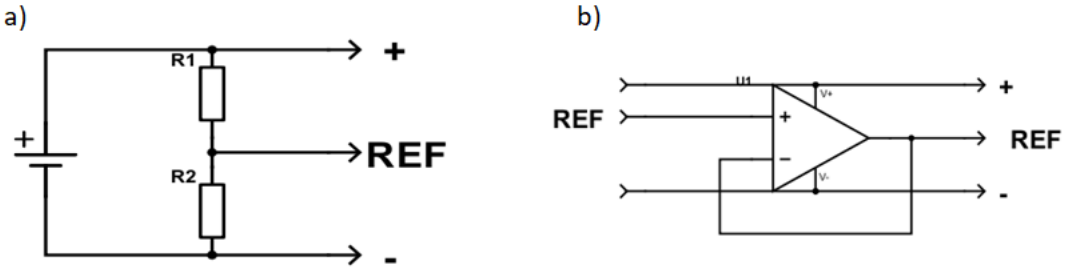


*Figure 36: a) Voltage divider. b) Opamp voltage follower with A = 1*

#### 4.2.9.2 Three-terminal fixed regulators

For the positive voltage regulators, we used 78xx series where the last two digits of the part number specify the output voltage, in our circuit it was 7809 and 7805. This voltage regulators can give up to 1A output current. For the negative voltage regulator, we used the 79xx series witch basically work the same way as the positive voltage regulators except for the negative output voltage. The voltage regulators are showed in Figure 35 as U2, U3 and U4.
When having a supply of both polarities like we have its recommended to have a pair of protection Schottky diodes (1N5817), showed as D4, D5 and D6 in the Figure 35. This prevents one of the supplies to bring the other one into reverse output voltage, which can cause a failure in the load or the regulator.
When choosing the additional capacitors, we chose capacitors over the recommended minimum, suggested by the datasheet (Fairchild, 2014) (Horowitz & Hill, 2015).

#### 4.2.9.3 Shutdown protection

If the regulator has a large capacitor at the output and the input voltage is brought to zero, for example with a short circuit the regulator can be damaged because the charged capacitance can source a destructive current back into the output terminal. To prevent this, we added a diode (1N4001) from the output to the input which will lead the destructive currents back to the input terminal, the diodes are showed as D1, D2 and D3 in Figure 35 (Horowitz & Hill, 2015).

### 4.2.10 Probe Design

Figure 37 shows the geometrical arrangement of the NIR light source (red) and the two detectors (yellow). The LEDs are placed in one end, and the two detectors follows in a straight line with the SSC being one centimeter from the source, which is the maximum distance recommended by Herold et. al. (2014) for a SC. The long channel is placed four centimeters from the emitter, which based on the work done in chapter 3.1.9, should give a sufficient cerebral contribution to the signal.

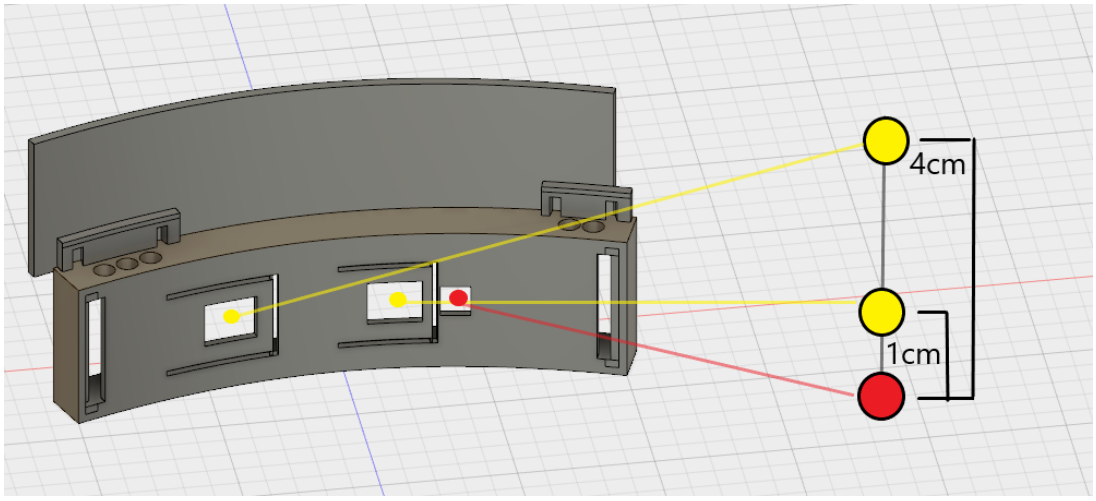


*Figure 37: Geometrical arrangement of the NIR light source and detectors.*

It is important that the source and detector are as close to the scalp as possible, while remaining perpendicular to the surface for optimal signal quality and penetration depth. To keep the S-D perpendicular to the surface, and at the same time provide an optimal fit for the head, the probe

was 3D printed in a flexible material which allows it to easily follow the curvature of the head (Figure 38). The flexible material is also softer than regular plastic, making the probe more comfortable to wear.

*Figure 38: Probe fitted on a head*

Because of the high amplifications needed to detect cerebral signals, it is important to keep the detectors clear from ambient light and light effects from other directions not perpendicular to the surface. To assure that the detectors do not saturate due to light contamination, the probe is lined with a thin copper tape (Figure 39) which reflects and absorbs most of the incoming light. This tape is also used to cover half of the detector surface on the SSC to prevent the internal transimpedance amplifier of the OPT101 to saturate. For fixation to the head, a Velcro strip was fastened on both sides of the probe, which provides length and tightening adjustment.

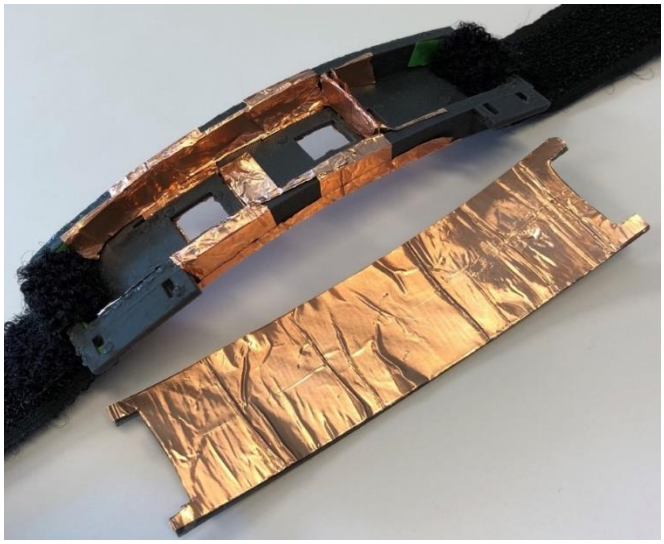

*Figure 39: Probe with copper-tape lining.*

### 4.2.11 PCB design

For PCB design we used Proteus professional 8, this is a program developed by Labcenter Electronic Ltd and are used for drawing schematics, PCB layout design and simulating. Proteus contains a big library of components and we were able to find close to every component we needed already in there, for those few components that did not exist we simply created the component schematic and PCB package directly in the program (Suresh, 2016).
When creating the PCB layout in proteus you can either have the program do it for you or draw it yourself. Because of the limits to our resources and the fact that the photodiodes had to be exactly 3cm apart we chose to draw it ourselves to get prints on only one side of our PCB and to get the measurements right.
On the main board and the power supply (Figure 40) we placed the components which needed to be close to each other manually, like decoupling capacitors and ICs (integrated circuits) and then used auto placer and auto router to automatically place the rest of the components and draw connection rails. On these cards we also chose to print on both sides to save space and for an even more compact PCB we chose to use some SMD components on the main circuit PCB.

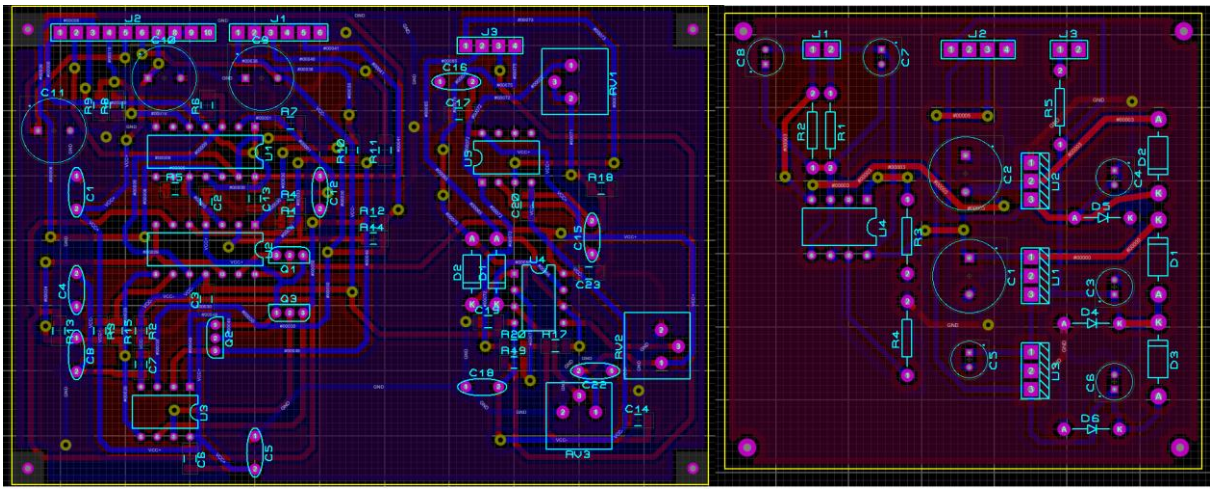

*Figure 40: PCB design. To the left; Main board. To the right; Power supply*

### 4.2.12 Etching the cards

To etch the card the first thing we did was to print the copper paths from proteus onto a clear sheet which was laid on top of a copper coated card before it was exposed to UV radiation to make a protection film on top of the copper. After this the card is washed in a bath with water and sodium hydroxide this will make the paths come to sight on the card. The last step is to wash the card with Iron-3-chloride 40% (FeCI) which will etch away the copper which was not highlighted from the sodium hydroxide. To get away the rest of the FeCl its washed in water then cleaned with acetone to remove the protection film before it is coated with a non-leading flux pen to make soldiering easier.

#### 4.2.13 3D printing

##### 4.2.13.1 Probe

The probe was designed using Autodesk Fusion 360, and printed on a Formlabs Form 2 3D printer with a flexible material (Figure 39).

##### 4.2.13.2 The instrument box

The instrument box was designed using Autodesk Fusion 360, and printed on Ultimaker 2+ 3D printer with PLA plastic material (Figure 41).

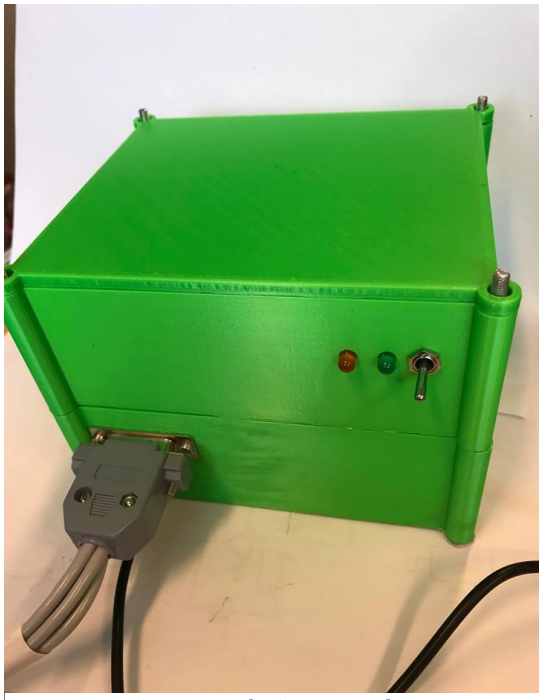

*Figure 41: The instrument box*

### 4.3 Safety measures

#### 4.3.1 fNIRS safety

There are three user safety aspect that were considered during the system design process:

- Dangers originating from supply voltages in the case off direct contact or short circuit.
- Dangers from tissue heating due to close proximity of NIR light emitters.
- Dangers of eye exposure to high intensity NIR light.

The system is designed for low power consumption and uses only low voltage components. A battery pack of ±9V dc ensures that the system is kept well under the allowed medical standard (IEC 60601-1) of 60 VDC when the accessible part of the system is kept under a cover that is accessible without the use of tools. In ordinary operation the electrical junctions of the NIR emitters and sensors is not in contact with the tissue, eliminating the need for galvanic isolation. Regarding eye exposure to NIR light, no safety standards currently exists for single wavelengths LEDs, but because LED light is not coherent, it should not pose any danger to the eye, even at relatively high intensities. As dangers from tissue heating go, two sources of heating occur: radiated energy from NIR light being absorbed by the skin, and conducted energy, which originates from the semiconductor junction of the LED. The temperature increase occurring from radiated energy is small, because NIR light is mostly absorbed by blood pigments and does no heat up due to constant circulation. According to Bozkurt et al., the main source of heating is due to the conducted energy from the semiconductor, and has been observed as high as 10°C and that "It is a well-known fact that the probability of cell death increases when the cell temperatures are sustained above 41°C. This value is also the limit value for pulse oximetry applications" (Bozkurt & Onaral, 2004). With the mean temperature of the arm being around 32°C and usually around 36°C on the forehead (Choi & Loftness, 2012), the maximum permitted increase in temperature is 9°C on the arm and < 6°C on the head during longer exposures to the semiconductor. The temperature increase can be minimized by avoiding direct contact with the skin, or, as is in our case, adjusting the radiance by sending the NIR light in short pulses (Bozkurt & Onaral, 2004).

## 4.4 Software

### 4.4.1 MATLAB

MATLAB R2017b is used to read serial data from the Genuino zero and to process and plot the data after testing. Using MATLAB, we programmed a Graphical User Interface (GUI), to facilitate the testing by controlling the Genuino Zero program through MATLAB, and to be able to perform data analysis through simple button clicks, instead of writing MATLAB commands. All the variables are stored in mat-files, making them easily accessible in the GUI at any point, as well as in the MATLAB workspace.

MATLAB has a support package for Arduino (MATLAB® Support Package for Arduino®) which supports a number of Arduino Boards, but not the Genuino Zero (MathWorks). Due to system requirements, the Genuino Zero was imperative. By using MATLAB's serial() function it was possible to set up serial communication between the Genuino zero and MATLAB without the support package. The serial() function, creates a serial port object associated with the specified port. Baud rate was set to 128000, which was the maximum baud rate of the serial port of the computer used for the programming. Tests showed that exceeding this baud rate caused problems with the data transfer.

#### 4.4.1.1 A general overview

The flow chart below (Figure 42) gives an overview of the functionalities in the GUI, and MATLABs response to user input.

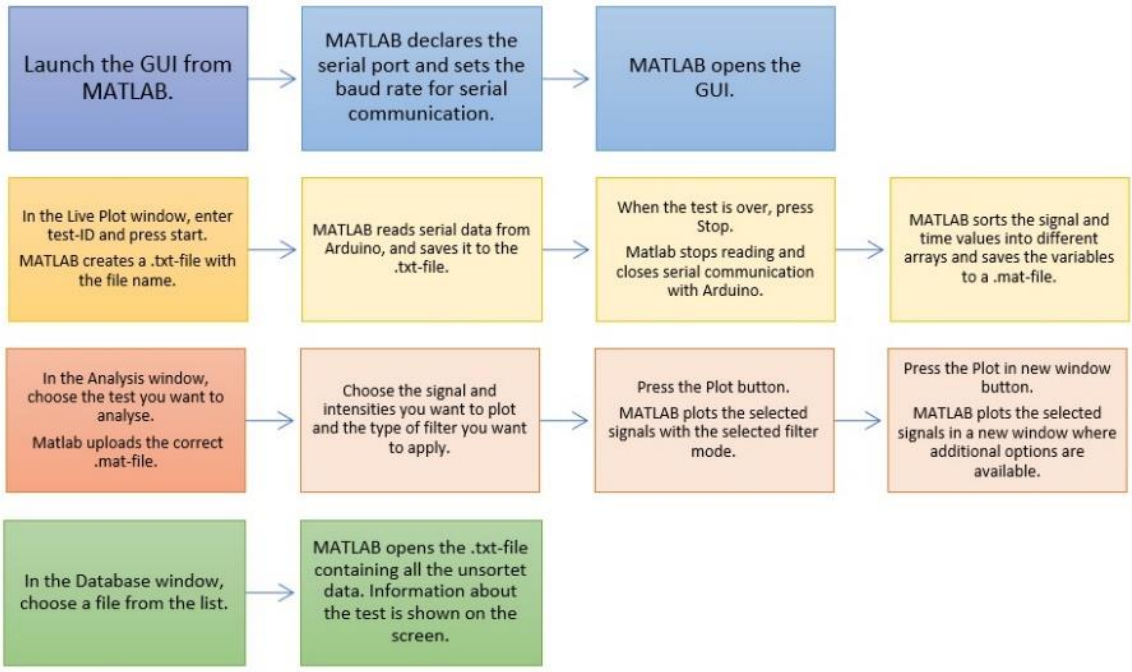


*Figure 42: GUI flow chart*

For a more extensive explanation of the GUI, see attachment IX.

#### 4.4.1.2 Data collecting and processing in the GUI

##### 4.4.1.2.1 The start-button callback function

The start button callback function is the function that performs the serial reading of the data sent from the Genuino zero. It depends on two other functions; the test-ID callback and the stop button callback. First, if a test-ID is not entered, and the start button is pressed, an error message will appear, and the program will not start. If a test-ID has been entered, the start button callback function will enter a serial-read while loop that runs until the stop button has been pressed. In order to allow the stop button callback to interrupt the start button callback, the while loop must contain a function that allows interruption. A callback will only allow interruptions from other callbacks if, firstly, the interruption property is enabled, and secondly it contains one of a set of specific functions that allow for interruptions to happen We used the pause() function to enable interruptions, and set it so small that the pause did not affect the speed (which is limited by baud rate).

##### 4.4.1.2.2 The data sorting algorithm

The data is saved in a txt-file, which is then divided into a time-array and a values-array. The same indexes of each array belong together, so the value of the time-array's $5^{th}$ index, belongs to the value of the values-array's $5^{th}$ index, and so on. The next step in the sorting algorithm is to sort the 15 different intensities within each wavelength/channel array. This means that each array is sorted into new 15 column arrays, each column corresponding to one intensity. The time arrays are again sorted accordingly, so the indexes still match. This means that the value

in for example row 329, column 4 in a values-array match the value in row 329, column 4 in a times-array. All the variables are saved to a mat-file with the test-ID as filename. The steps in the sorting function can be seen in attachment X. For a schematic description of the data sorting algorithm, see attachment X.

#### 4.4.1.2.3 Plotting

Our initial idea was to live plot the signal as it was read from the Genuino zero, but tests proved this to be very time-consuming task. We tested different plotting options by making a simple Arduino program that read different values at the analog input and sent them to serial output. We then made a program for reading serial input in MATLAB, and timed the process first without plotting, and then with different plotting functions. The results can be seen in Table 5.

*Table 5: MATLAB live plot speed testing*

| ***Line type*** | **No plotting** | **animatedline** | | **plot** | |
|---|---|---|---|---|---|
| ***Plotting function*** | | *drawnow;* | *drawnow limitrate;* | *drawnow;* | *drawnow limitrate;* |
| *Number of scans* | 3500 | 3500 | 3500 | 3500 | 3500 |
| *Time* | 3.3721 | 91.3607 | 11.4298 | 736.8179 | 27.0421 |
| *Scans per second* | 1037.93 | 38.31 | 306.22 | 4.75 | 129.43 |

These data show that the plotting process significantly slows down the process, and to be able to read data as quickly as required, we decided not to live plot the data, but write it directly to file, sort the data in MATLAB and plot the unfiltered data after the serial reading was finished.

The processed and filtered data can be plotted in the GUI tab 2. The plot button callback function reads the data from the list box, and all the different check boxes, which provide information about what the user wants to plot. It uses the data to apply the correct filter and plot the selected signals. The filters are specified in chapter 4.5.

### 4.4.2 Arduino

#### 4.4.2.1 Speed testing

Getting a certain accuracy of sending the data, as well as reading and receiving it is vital in a circuit that handles data acquisition. Initial testing of the functions included in the Arduino IDE libraries (see attachment VIII), showed that the speed of some of these functions was slower than expected. Some of which were the “digitalRead()” and the “analogRead()” functions, which initially was used for switching the 4066 switch and for sending sensor readings back to the serial port and MATLAB. The performance of some functions can be seen in Table 6.

*Table 6: Arduino speed tests (see attachment VIII)*

| **Function name:** | **AnalogRead** | **AnalogWrite** | **DigitalRead (true C)** | **If-statement** | **Micros()** | **Println of int** |
|---|---|---|---|---|---|---|
| **Time [µs]:** | ~440 | ~7 | ~4 | ~6 | ~4 | ~23 |

To continue using easily available functions in Arduino, it was decided to measure the expected time the functions used and let this be the guide in deciding at which frequency to acquire sensor data. The most limiting function among the Arduino functions, was without doubt the "analogRead", as seen in Table 6. This function needed approximately 440 µs, and for each intensity increment (as illustrated in Figure 43) it was needed to make two readings, one for long and one for short channel. Having a minimum of 960 µs each loop (see attachment VIII), a period of approximately 1000 µs with the minimum of necessary functions would ideally be possible. Some additional functions were needed, and 66.7 readings pr. second for each channel is not needed for measuring hemodynamic changes. After including all functions needed, an oscilloscope test was made to measure the frequency of the signal (Figure 43).

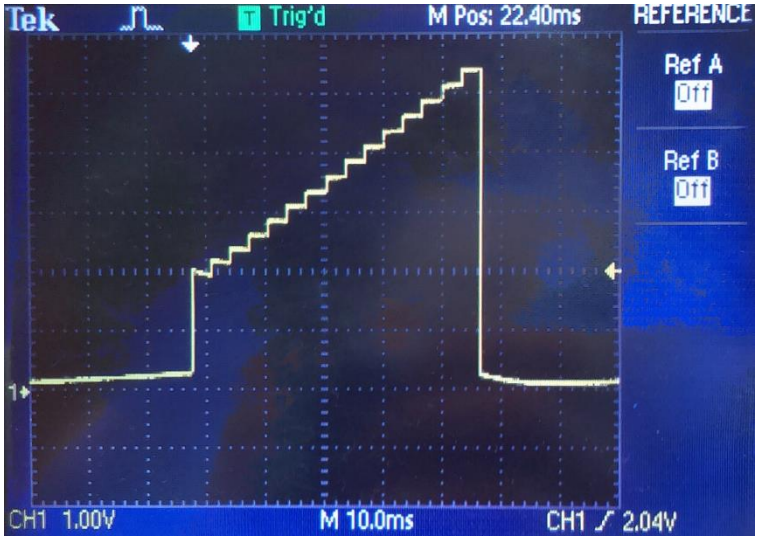


*Figure 43: Oscilloscope frequency test*

The period of each wave is, as seen in Figure 43, is 48 ms. This means a period of each increment (and sensor reading) of $\frac{48\text{ ms}}{15} = 3.2\text{ ms}$, and $\frac{1\text{ s}}{48\ ms} \approx 20.8\ readings$ for each intensity of each channel per second.

## 4.5 Data processing

### 4.5.1 Digital outlier filter

Sometimes the signal will contain outliers. Outliers have in common that they are far away from the main part of the signal and only contains a few samples. These are obvious noise and because of their extreme values, they will affect the average filtering to a large extent. Therefore, it is important to remove them and why it is important to do it before further filtering. To remove the outliers, we chose to use MATLAB's Hampel filter. The Hampel filter, as opposed to MATLAB's filloutliers filter, looks at a window of x samples at a time, instead of the entire signal. In this way, it eliminates the outliers that are within the "frame" of the signal but clearly an outlier when looking at the neighboring samples. MATLAB describes the Hampel filter as following:

"y = hampel(x) applies a Hampel filter to the input vector, x, to detect and remove outliers. For each sample of x, the function computes the median of a window composed of the sample and its six surrounding samples, three per side. It also estimates the standard deviation of each sample about its window median using the median absolute deviation. If a sample differs from the median by more than three standard deviations, it is replaced with the median. If x is a matrix, then Hampel treats each column of x as an independent channel." (Mathworks, n.d.). An illustration of window length is shown in Figure 44.

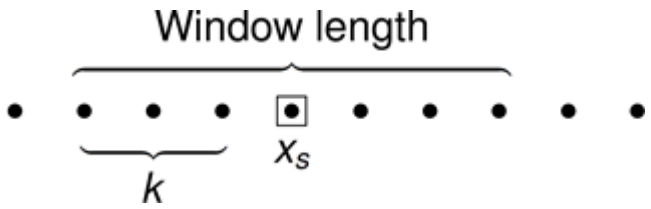


*Figure 44: Illustration of window length (Mathworks, n.d.)*

We have landed on the default value of three samples on each side of x, if desired, this can be changed by adding a value k behind the x. Y = hampel(x,k). An example is shown in Figure 45.

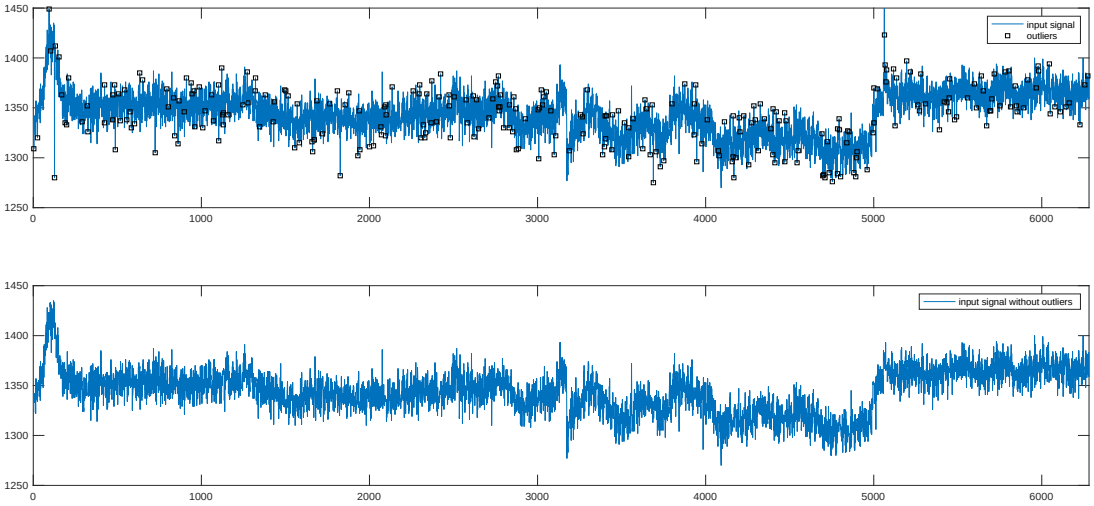


*Figure 45: With and without outlier filter*

### 4.5.2 Lowpass- and bandpass filtering

Many different filters have been applied to fNIRS signals in different studies, but so far, there have been no reports of any type of filter having a clear advantage over another (Naseer & Hong, 2015). We opted for a lowpass filter with adjustable cut-off frequency, and we also have the opportunity in the GUI to apply a bandpass filter with a lower cut-off frequency of 0.01 Hz and an adjustable upper frequency. The default cut-off frequencies were set to 0.5 for the lowpass, and 0.1 for the bandpass upper cut-off (Naseer, Hong, & Hong, 2014)

Experimental errors, such as motion artifacts, which can result in a spike-like noise can be removed in several different ways, for example spline interpolation, wavelet transform and Kalman filtering (Gagnon et al., 2012). As explained above, we used a MATLAB hampel filter to remove these spikes.

Further, a lowpass filter will efficiently remove instrumental noise, that is noise from the instrument and from the surroundings. A cut-off frequency of 3-5 Hz has reportedly removed such noise successfully (Naseer & Hong, 2015). We applied a $5^{th}$ order Butterworth lowpass filter, with a cut-off frequency of 0.5 Hz by default, but this can be changed in the GUI. Figure 46 shows the unfiltered and the lowpass-filtered signal.

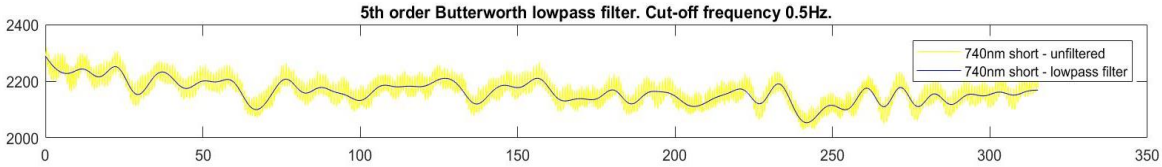


*Figure 46: Lowpass-filtered signal*

At last, a second order Butterworth bandpass filter with lower cut-off frequency of 0.01 Hz and upper cut-off frequency of 0.1 Hz as the default filter in the GUI. The upper cut-off frequency order can be changed in the GUI by the user. The lower frequency of 0.01 Hz will remove the DC component of the signals. The result is shown in Figure 47.

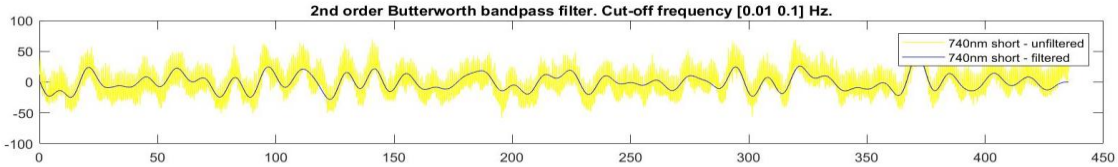


*Figure 47: Bandpass-filtered signal*

The relatively low upper cut-off frequency of the bandpass filter will remove pulse artifacts, which usually appear with a frequency of around 1-2 Hz. Bandpass filtering cannot be used when the physiological noise frequencies overlap with the hemodynamic response signal, for example noise caused by respiration. Other methods, such as adaptive filtering, may be applied to overcome this issue (Naseer & Hong, 2015).

### 4.5.3 Post-processing

To be able to analyze the data in protocol 2, we needed 1 averaged graph for each of the 4 channels for each difficulty (12 graphs). To get the averaged data, the following has been done to the raw data:

1. Valid intensity
   Below is a table of which intensity being the highest which did not reach saturation. The lowest of these intensities for each channel and each difficulty is the valid intensity.

*Table 7: Overview of the highest intensities where the sensors does not go in saturation where the valid intensity is in bold.*

| Difficulty | Person number | 740 nm short | 740 nm long | 855 nm short | 855 nm long |
|---|---|---|---|---|---|
| 1 | *1* | 15 | **15** | 6 | **15** |
| | *2* | **11** | **15** | **4** | **15** |
| | *3* | 15 | **15** | 5 | **15** |
| 2 | *1* | 15 | **15** | 6 | **15** |
| | *2* | **11** | **15** | **4** | **15** |
| | *3* | 15 | **15** | 6 | **15** |
| 3 | *1* | 15 | **15** | 6 | **15** |
| | *2* | **12** | **15** | **4** | **15** |
| | *3* | 15 | **15** | 5 | **15** |

2. Critical samples
   Genuino sends 207 - 209 samples during each 20-second test and 153 - 155 samples during each 15-second break but varies a bit more in the 2-minute break at the beginning of each of the tests. To make the analysis as exact as possible we checked the time Genuino sends to MATLAB to find the exact sample where the first 2 minutes have passed, after that we added 208 samples for each test and 154 for each break.

*Table 8: Overview of which sample happens at 2 minutes*

| ***Difficulty*** | | **1** | | | **2** | | | **3** | | |
|---|---|---|---|---|---|---|---|---|---|---|
| *Person number* | | *1* | *2* | *3* | *1* | *2* | *3* | *1* | *2* | *3* |
| **Sample number** | *2 minutes* | 1280 | 1266 | 1241 | 1291 | 1274 | 1268 | 1298 | 1276 | 1275 |

3. Butterworth filter
   Applied the Butterworth filter to the data.

4. Baseline
   To find the baseline we chose the valid intensity and found the average value of the 2 minutes rest phase at the beginning of each of the filtered tests. (See attachment VII, Protocol 2)

5. Normalization
   To normalize the different tests, we attracted the baseline from the data at the valid intensity.

6. Averaging
   For each test, we took out the 6 active parts from the normalized data by using the Critical samples. For each difficulty, the 6 tests from each person was added together and divided by 18.

# 5 Results and evaluation

## 5.1 Composition of final product

### 5.1.1 Instrument box

The instrument box was created with two sections, consisting of the top section which contains the batteries and the power supply, and the bottom section which contains the main circuit and the Genuino Zero. For simplicity, and the possibility to easily add more probes, a DB15 contact was added between the probe and main circuit for easy connection. The instrument box with the probe can be seen in Figure 48.

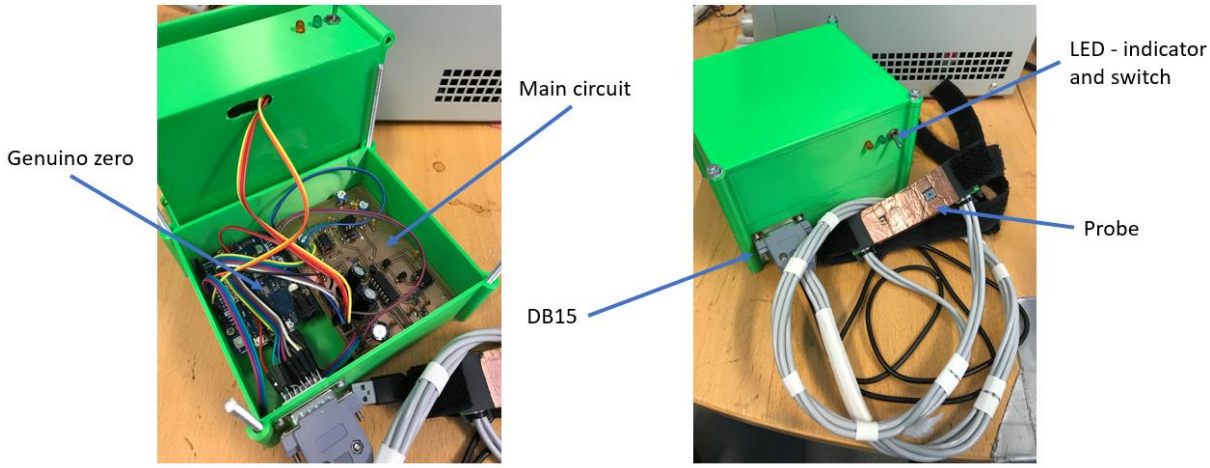


*Figure 48: The assembled product*

### 5.1.2 The probe

When designing the probe, several challenges were encountered. Through the process of finding a good design, many prototypes (Figure 48) were made before ending up with the flexible curved probe. Another challenge that was encountered was that the plastic material used in the 3D printers were close to transparent to near-infrared light, which means the detectors would read the light signal directly from the source LED. The solution to was to find a material which would not let the near-infrared light pass directly throught to the detector. The material used was copper tape, in which the inside and outside of the probe was covered (see Figure 51). All of this is explained in detail in chapter 4.2.10.
There were made three separate PCBs which was fastened inside the probe. One for the two LEDs, and one for each of the photodiodes. The reason for this was the curved probe, so that the LEDs and both detectors would be in contact with the skin at all times.

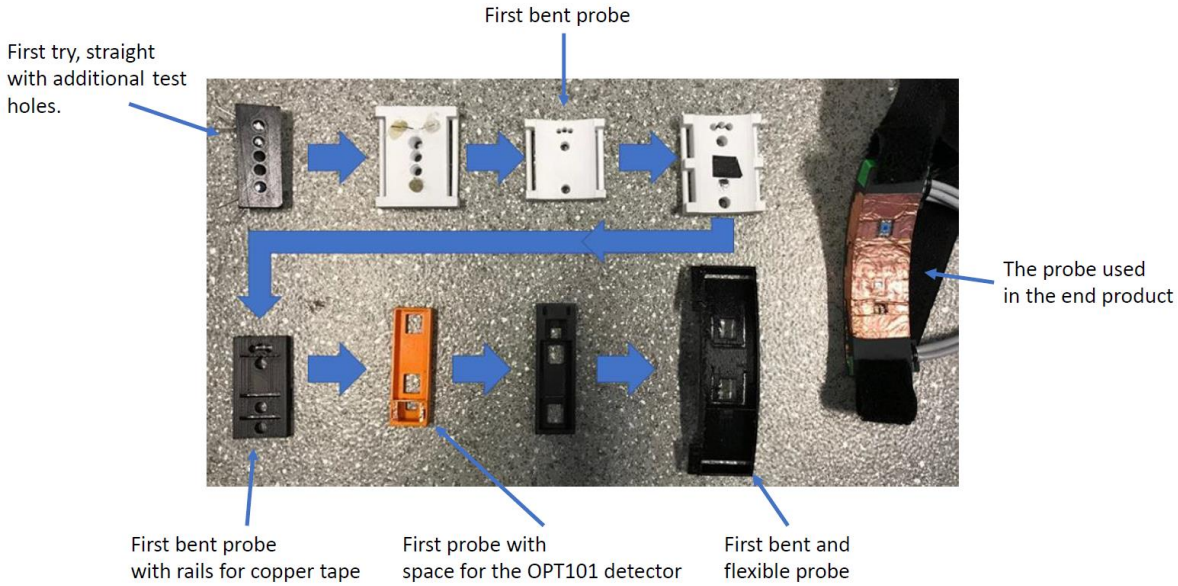


*Figure 49: The history of the probe designs*

### 5.1.3 Electrical circuitry

#### 5.1.3.1 Long channel amplification and filtering

As explained in chapter 4.2.7.1, a potentiometer was added to manipulate the additional amplification of the signal returning from the long channel photodiode. The amplification used during the protocols are noted in the protocol forms (see attachments XII and XIII) but the additional amplification for the long channel was commonly set to be 71.

#### 5.1.3.2 Power supply

When designing the power supply, some difficulties were encountered. One challenge was a voltage drop when the load (main circuit) was active, which made a significant difference in load on negative and positive rail. The reason to this was the opamp's inability to provide enough current to stabilize the differences on the positive and the negative rail. As explained in chapter 4.2.9, a second opamp was implemented which made the power supply able to handle the load.
Another issue was which size of bypass capacitors to use for the voltage regulators. To make sure that potential momentary spikes and drops in voltage would be removed, 1000 µF capacitors were added. The capacitors used exceeds the minimum recommendation from the datasheet (Fairchild, 2014).
To control the power supply, a power switch and a LED indicator was added.

## 5.2 Short channel

One of the main goals of this project was to test if a SSC could be added as a regular PD without saturating by regulating the intensities of the emission sources (Figure 50).

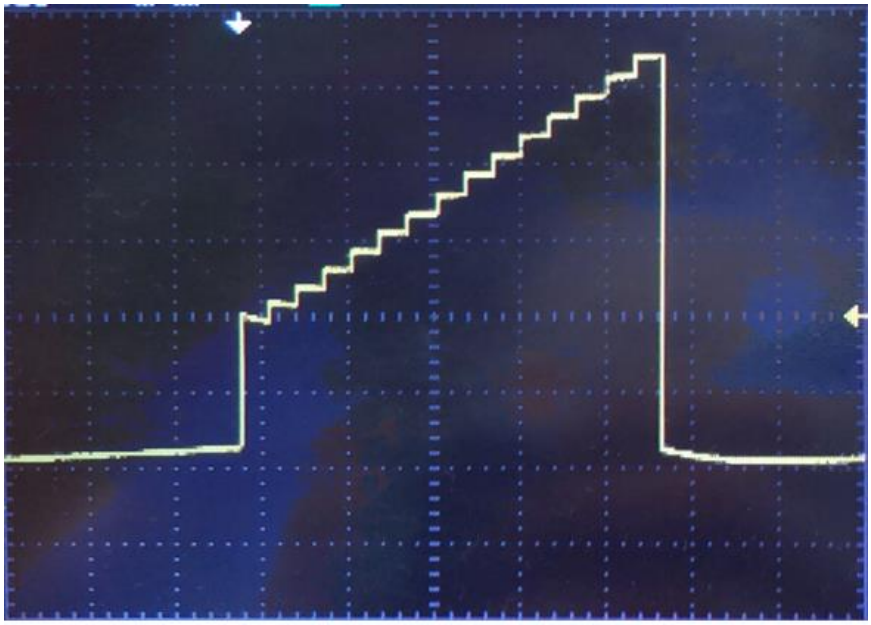

*Figure 50: The signal used for amplitude modulation on the LEDs. This results in 15 different intensities on the LEDs*

The sensor is also partially covered in copper tape to limit photons from hitting and saturating the detector (Figure 51).

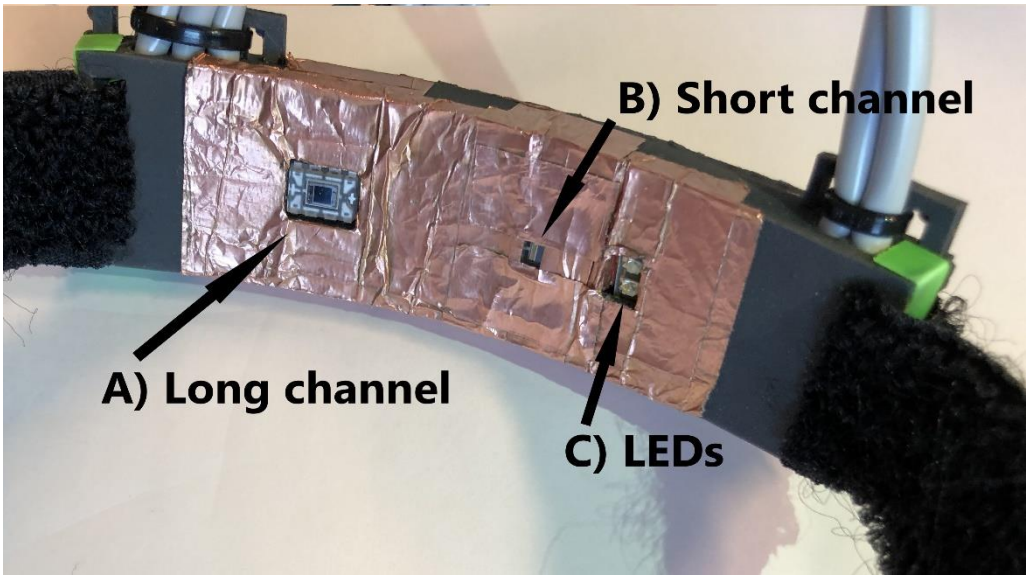


*Figure 51: Picture of probe. A: Long channel B: Short channel (partially covered to limit photons) C: Light emission sources*

Figure 52 shows the results from a protocol 1 test where the first 5 intensities does not saturate the detector.

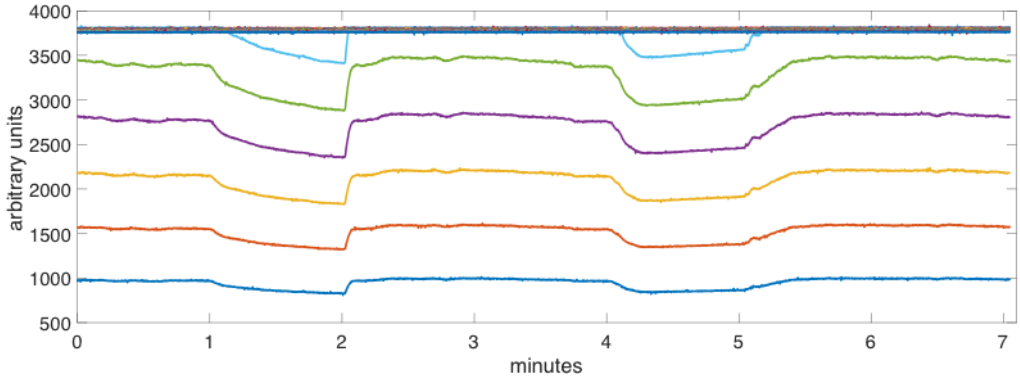


*Figure 52: Short channel results from cuff test. Emission source: 740nm*

## 5.3 Graphical User Interface

The Graphical User Interface for our instrument is a MATLAB function that upon launch will open a tabbed window containing three tabs, each with its own specific functionality. Tab 1 is the Test tab, in which the test response data is read and saved in a .txt-file that MATLAB then uses for data sorting. Live plotting, live display of the test time and the possibility of choosing test protocols are functionalities that can be added to increase the usability of the product.

In tab 2, the Analysis tab, the most recent or any of the previous tests can be plotted in both filtered and unfiltered versions, see Figure 53.

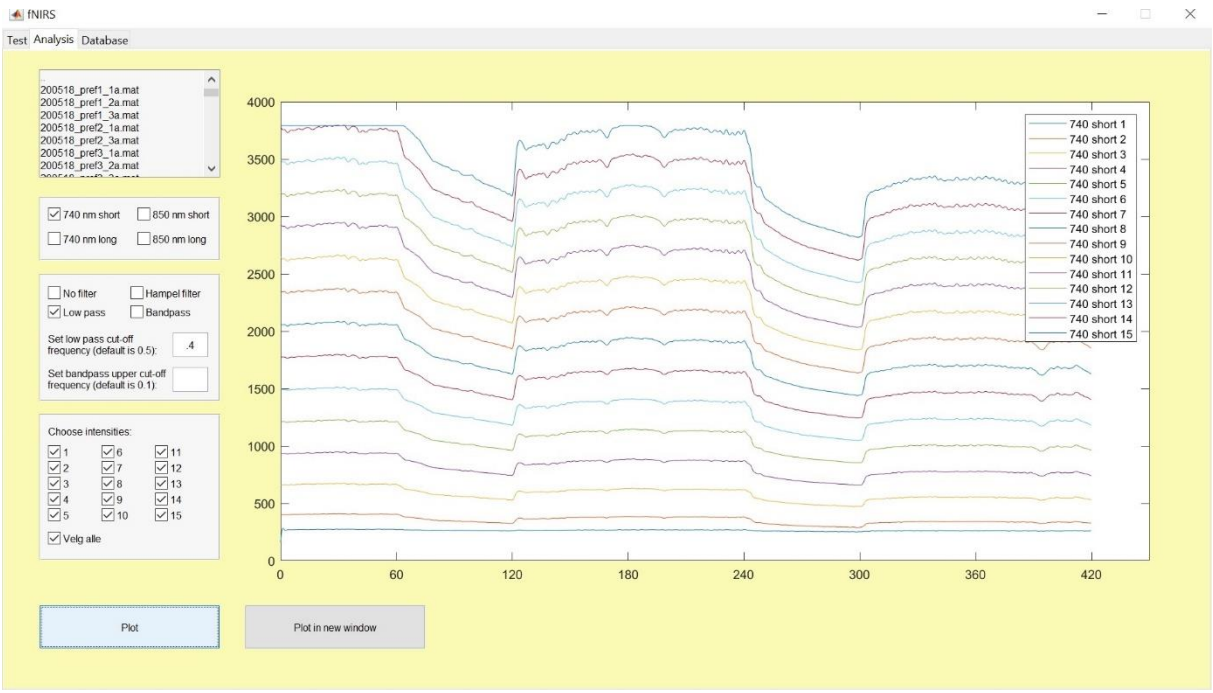


*Figure 53: The GUI "Analysis" tab*

Filter cut-off frequencies can be changed here, and the responses can be plotted, either one at a time, all together or a selected few. All the plots can also be opened in a MATLAB figure window, where all the MATLAB plot property options are available. At present, only one test file can be accessed at a time, which puts a limitation on the data analysis as cross-test

comparisons are not possible in the GUI at this point. These analyzes can still be performed, however, as all the .m-files containing all the sorted data are stored and can be opened in the MATLAB workspace. A natural next step in the GUI function would be to implement this possibility here as well.

The third tab, the Database tab, contains a list box which displays all the .txt-files that contain the raw data. They can be opened from the GUI, and key information about the selected test is displayed on the screen.

## 5.4 Test protocols

To verify that the instrument records physiological information, the tests outlined in chapter 4.1 were performed on several volunteers.

### 5.4.1 Test protocol 1

The data collected in this test protocol is obtained from the sensor being placed at right arm of the test subject, as described in chapter 4.1.1. In Figure 54 we see the expected NIRS response when a cuff is placed on arm and used to block the blood flow, this experiment was conducted by Jaafar et. al. (2014).

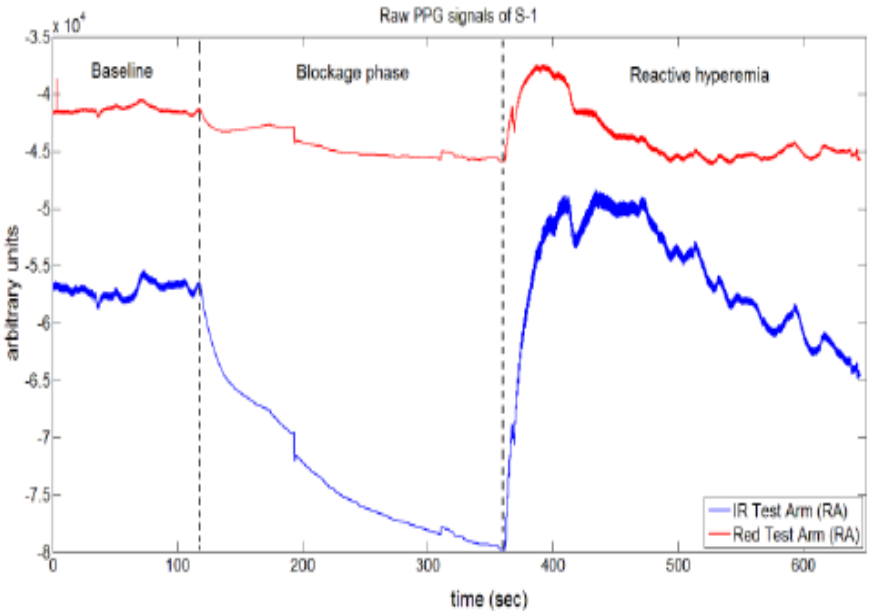


*Figure 54: Results from cuff test on arm. Red: Spectroscopy measurement with red LEDs. Blue: IR measurements.(Jaafar, Zahedi, & Ali, 2014).*

Figure 55 shows the raw NIRS measurements obtained from our system on a similar test. We can see that the results are comparable. The reduction in signal intensity is due to hemoglobin being trapped in the arm when the cuff is tightened. We observe that the signal goes rapidly back to baseline after a small overshoot, which is also an expected response (Jaafar et al., 2014).

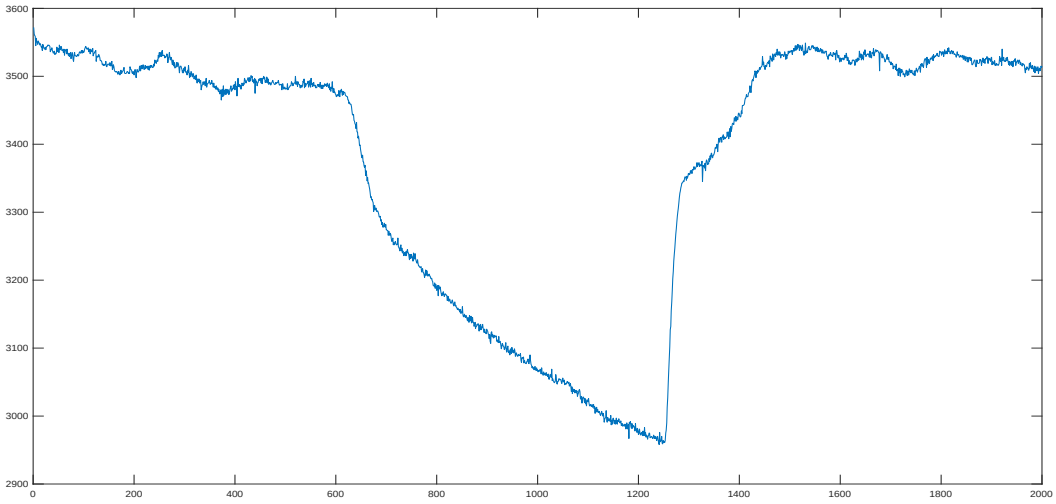


*Figure 55: NIRS response from our system when a cuff is tightened on an arm*

### 5.4.2 Test protocol 2

The data collected in this test protocol is obtained from the sensor being placed at the test subject's forehead, corresponding to BA10. In Figure 56 the data of each plot corresponds to one channel reading one wavelength, being an average of the response from 6 tasks of equal difficulty performed by three different people.

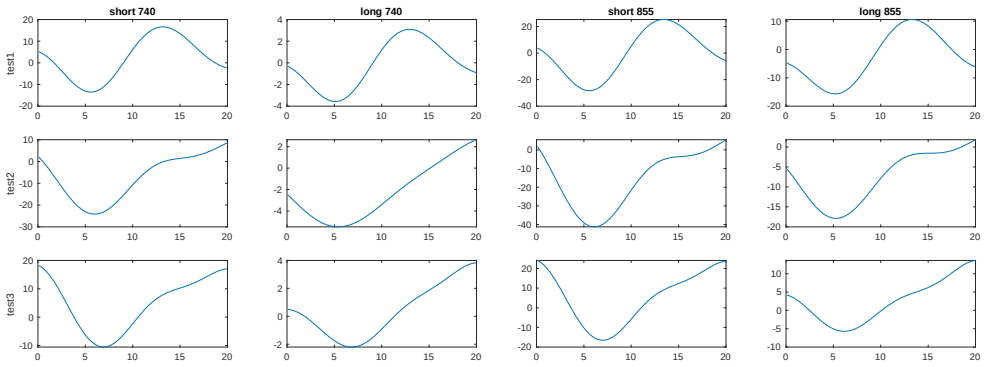


*Figure 56: Results from test protocol 2 with baseline as 0. The x-axes are seconds and the y-axes are arbitrary units.*

### 5.4.3 Control study

There was not conducted a control study to validate or invalidate our findings, but it would've been preferred to control our readings to the same protocol tests done during (e.g.) a fMRI study. This would have concretized our findings, as because of a number of error sources (which will be discussed in 5.5) our findings in prefrontal cortex readings cannot be concluded to be certain.

## 5.5 Error sources and observations

### 5.5.1 Software

- Issues regarding the choice of the baud rate for the Genuino and MATLAB was met during testing. These issues were resolved when baud rate was matched with the maximum listed baud rate for the serial port of the PC. A few errors (missing values) did occur even after this matching but has not occurred as a systemic error.

- During one of the test protocols the timing values received from the Genuino restarted and began sending values starting from zero. This occurred after a longer period of testing, and the issue was the micros() function used for timing in the Genuino zero. This function restarts after approximately 70 minutes (Arduino, n.d.-b) and therefore after continuous testing for more than 70 minutes, restarted.

### 5.5.2 Hardware

- As mentioned in Table 2, one drawback of using LEDs as an emission source is that the light is not totally monochromatic. The light varies in color depending on the relative intensity applied to LED (Figure 57). This can pose a problem if the relative changes in oxy- and deoxyhemoglobin is calculated using the MBLL, as this is a wavelength dependent equation.

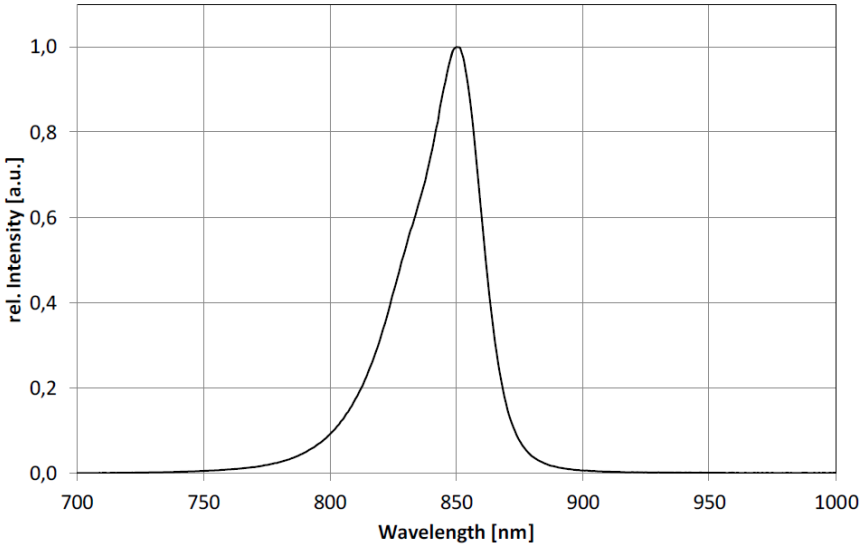


*Figure 57: The spectral bandwidth of the OIS-330 IT855 (OSA opto light, 2012)*

### 5.5.3 Test protocols and artifacts

During our pilot studies and preliminary test protocols we encountered a number of error sources and artifacts in the measurements and in our preliminary protocols. Following is a list, some with pictures, of the most important sources of error that we encountered:

- The cables connecting the instrument and the probe are *sensitive to movement* and gave clear spikes in the measurements. Therefore, minimizing movement during the test was vital. As seen in Figure 58, motion of the cables will disturb the signal.

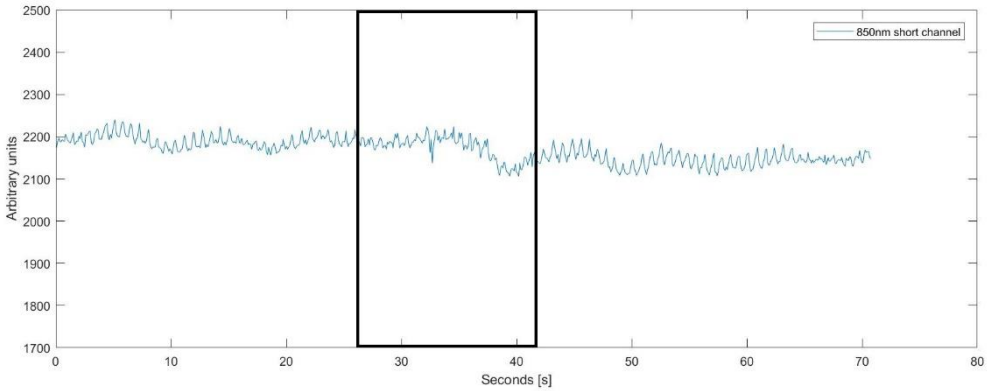


*Figure 58: Cable motion artifact*

- During prefrontal cortex tests we saw significant spikes due to *movement/wrinkling of the forehead*, as seen in Figure 59. In conversations with a psychologist that has performed tests with professional fNIRS instruments we were told that this is a frequent problem with several fNIRS instruments. To minimize these effects, we placed the probe higher on the forehead, just below the hair line, as well as telling the subject to avoid any such movements during the test.

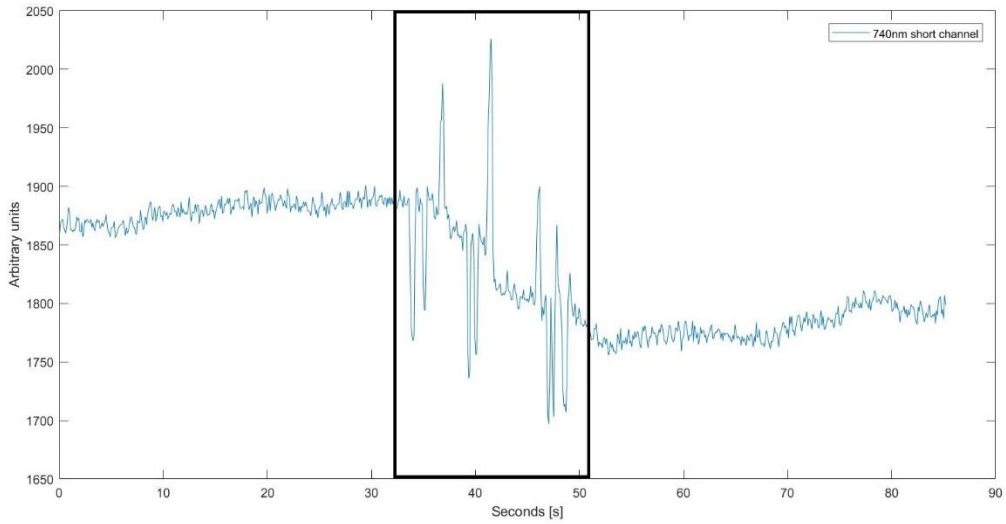


*Figure 59: Forehead wrinkling artifact*

- In preliminary testing of the prefrontal cortex protocol, a test where the subject would name all cities starting with a given letter was tested both verbally and non-verbally. Here we saw that during the non-verbal test, all trends that were visible during the verbal test were completely gone. This indicating that *the voice of the subject* alone would affect the sensor readings to such a degree, we decided to have all the protocols non-verbal to eliminate the effects this had to the sensor readings. Vitorio et. al. also reports

on this specific artifact, saying: “Talking results in task related low frequency artefacts with a frequency similar to the hemodynamic response and is more pronounced in anterior channels (prefrontal cortex)”.

- *Ambient light* makes a significant difference to the offset of the readings. A change in ambient light would therefore severely affect the validity of the readings. An important precaution is to assure that the ambient light stays constant during the reading, which includes that the test subject stays in the same position and does not move unnecessarily much during the test. As seen in Figure 60, the offset varies accordingly to ambient light. On each side of the orange square, the ceiling lights were turned on, and within the orange square the blinds covering the window was opened as well.

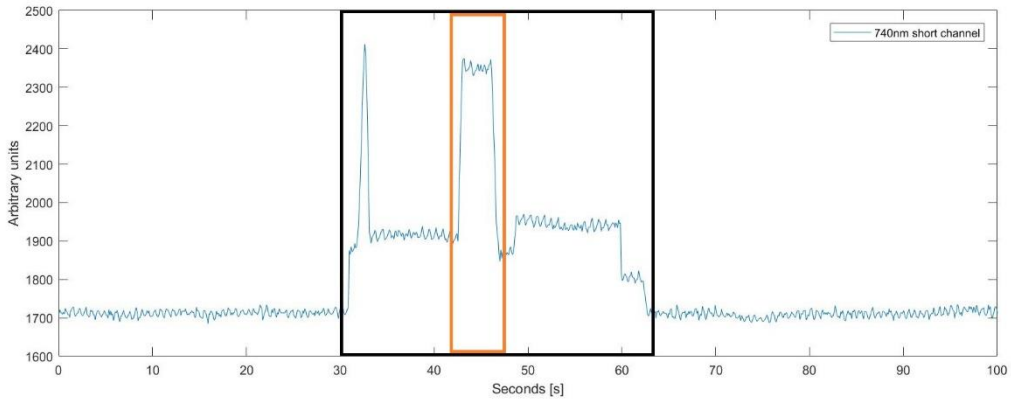


*Figure 60: Ambient light artifact*

- *Pulse artifacts* follows the signal like an oscillation during the whole reading session. These were not considered a problem as the pulse artifact disappears after the signal is filtered in MATLAB, as explained in chapter 4.5.2. In Figure 61, the pulse in this instance can be calculated to $\frac{12\ beats}{10\ s} \cdot 60\ s = 72\ \frac{beats}{min}$. This was controlled with a Nokia Steel HR wristwatch, and was shown to have an accuracy of $\pm 4 \frac{beats}{min}$.

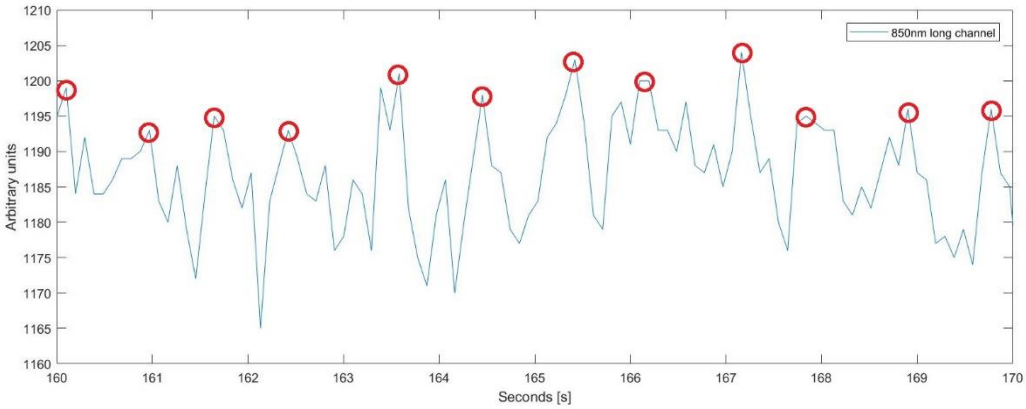


*Figure 61: Pulse artifact*

- An artifact that we have not observed, but was advised to account for in a conversation, is that the response could be affected by the *presence of any other persons* in the room. To handle this, the two persons that are present, will stay outside of the test subjects

visual field to minimize any effect that their presence could have on the test subject during the test.

- *Hair* adds a lot of noise as well as making it difficult to get good readings. During the pilot studies it was tried to establish a test protocol for reading from the occipital lobe, visual area 1. Because this area is covered with hair and made it hard for us to see any significant trends, we decided to stay with a test protocol covering only areas not covered by hair.

## 5.6 Graphical User Interface

The Graphical User Interface for our instrument is a MATLAB function that upon launch will open a tabbed window containing three tabs, each with its own specific functionality. Tab 1 is the Test tab, in which the test response data is read and saved in a .txt-file that MATLAB then uses for data sorting. Live plotting, live display of the test time and the possibility of choosing test protocols are functionalities that can be added to increase the usability of the product.

In tab 2, the Analysis tab, the most recent or any of the previous tests can be plotted in both filtered and unfiltered versions, see Figure 62.

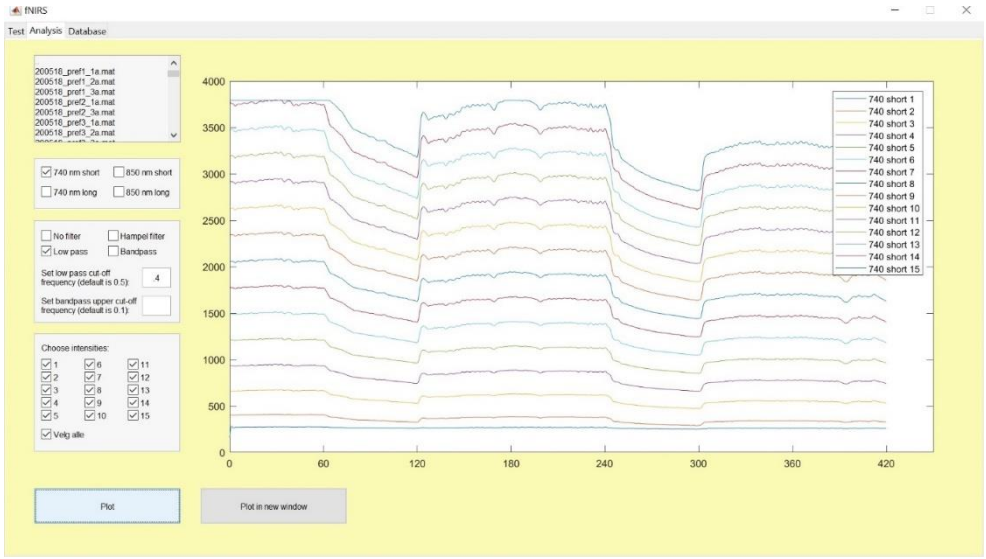


*Figure 62: The GUI "Analysis" tab*

Filter cut-off frequencies can be changed here, and the responses can be plotted, either one at a time, all together or a selected few. All the plots can also be opened in a MATLAB figure window, where all the MATLAB plot property options are available. At present, only one test file can be accessed at a time, which puts a limitation on the data analysis as cross-test comparisons are not possible in the GUI at this point. These analyzes can still be performed, however, as all the .m-files containing all the sorted data are stored and can be opened in the MATLAB workspace. A natural next step in the GUI function would be to implement this possibility here as well.

The third tab, the Database tab, contains a list box which displays all the .txt-files that contain the raw data. They can be opened from the GUI, and key information about the selected test is displayed on the screen.

# 6 Conclusion

This section offers concluding remarks as well as recommendations for future development of the project.

## 6.1 Conclusion

The goal of this project was to develop a working fNIRS instrument for measuring brain activity using three different wavelengths, as well as reading and analyzing the data acquired from it. A key element was to use an amplitude modulated signal to meet the challenges of SC saturation.

These goals were reached, except that the third wavelength was not implemented due to shipment delays. The instrument, however, is designed for implementation of a third wavelength at a later point.

The result is a working fNIRS instrument that measures light attenuation through brain tissue by way of an amplitude modulated signal measured at two different source/detector distances. A custom designed graphical user interface made in MATLAB facilitates data reading and processing and can easily be adjusted to include more analysis options in the future.

Several tests were performed that showed a significant trend in all test subjects related to blood volume changes in the brain during cognitive activities, a result which is comparable to previous studies. This verifies the functionality of the product.

## 6.2 Recommendations for future work

- Replace the batteries with rechargeable, longer lasting batteries.
  One of the advantages of fNIRS is the potential portability of the instruments. With this in mind, longer-lasting batteries would be beneficial to be able to conduct more and/or longer tests before the batteries needs to be recharged.

- Make it possible to power device directly through the wall socket.
  Having the possibility of powering the instrument directly through the wall socket is also practical for when the instrument is used in a stationary manner, or as a back-up solution if the batteries run out.

- Replace the current LEDs with the LEDs described in section 4.2.4.
  This will make it possible to measure other chromophores than hemoglobin.

- Print the probe on a flexible PCB.
  This will make it possible to only have one PCB in the probe rather than three separate, which is the current design.

- Add more channels to the instrument.
  Adding more channels to the instrument will increase the amount of data and will also make it possible to measure in several locations at a time.

- Apply the modified Beer-Lambert law to the acquired data.

  Applying the modified Beer-Lambert law to the data will hopefully reveal information about the varying levels of oxy- and deoxyhemoglobin in the blood during cognitive tasks.

- Analyze the correlation between the short and long channel signals and develop an algorithm for using the SC data for regression filtering.

  This is an interesting area of study for future signal processing in fNIRS and would make for a very exciting next step.

- Battery monitoring

  It would be beneficial to add a way to monitor how much power there is left in the batteries, and possibly an estimate of how much time left of use.

- Expand the GUI functionality

  Adding more filtering options will make data analysis even easier. Short and long channel correlation, as mentioned above, could also be analyzed through the GUI.

# 7 Literature


Abramowitz, M., & Davidson, M. W. (n.d.). Photomultiplier Tubes. Retrieved from https://www.olympus-lifescience.com/en/microscope-resource/primer/digitalimaging/concepts/photomultipliers/

Ainslie, P. (2012). *Applied Aspects of Ultrasonography in Humans*. In (pp. 198). Retrieved from https://www.intechopen.com/books/applied-aspects-of-ultrasonography-in-humans doi:10.5772/1113

Allen, M. D., & Fong, A. K. (2008). Clinical application of standardized cognitive assessment using fMRI. I. Matrix reasoning. *Behav Neurol, 20*(3), 127-140. doi:10.3233/ben-2008-0223

Amirlak, B. (2017, November, 29). Skin anatomy. Retrieved from https://emedicine.medscape.com/article/1294744-overview

Arduino. (2018). Serial. Retrieved from https://www.arduino.cc/reference/en/language/functions/communication/serial/

Arduino. (n.d.-a). GENUINO ZERO. Retrieved from https://store.arduino.cc/genuino-zero

Arduino. (n.d.-b). micros(). Retrieved from https://www.arduino.cc/reference/en/language/functions/time/micros/

Arthurs, O. J., & Boniface, S. (2002). How well do we understand the neural origins of the fMRI BOLD signal? *Trends in Neurosciences, 25*(1), 27-31. doi:https://doi.org/10.1016/S0166-2236(00)01995-0

Avago. (2015). HLMP-3301, HLMP-3401, HLMP-3507, HLMP-3762, HLMP-3862, HLMP-3962, HLMP-D401
T-13/4 (5 mm) Diffused LED Lamps. Retrieved from http://www.farnell.com/datasheets/1918235.pdf?_ga=2.100495514.569044879.1526729325-127602487.1516187345&_gac=1.120567034.1526758511.Cj0KCQjwlv_XBRDrARIsAH-iRJSi8j7GSEhcO3NVpt6iUFhNNM4udbIVPsiOlMIvjFV2V6-m1nJITe0aAvKJEALw_wcB

Bakker, A., Smith, B., Ainslie, P., & Smith, K. (2012). *Near-Infrared Spectroscopy*.

Baric, L., Stupin, A., Bari, F., & Drenjancevic, I. (2013). *Reproducibility of post-occlusion reactive hyperaemia assessed by laser Doppler flowmetry in young healthy women* (Vol. 116).

Barth, M., & Poser, B. (2011). *Advances in high-field BOLD fMRI* (Vol. 4).

Boas, D. A., Dale, A. M., & Franceschini, M. A. (2004). Diffuse optical imaging of brain activation: approaches to optimizing image sensitivity, resolution, and accuracy. *NeuroImage, 23*, S275-S288. doi:https://doi.org/10.1016/j.neuroimage.2004.07.011

Bochenkov, V., & Sergeev, G. (2010). *Metal Oxide Nanostructures and Their Applications* (Vol. 3): American Scientific Publishers.

Bohren, C. F., & Huffman, D. R. (1983). *Absorption and scattering of light by small particles*. New York: Wiley.

Bozkurt, A., & Onaral, B. (2004). Safety assessment of near infrared light emitting diodes for diffuse optical measurements. *BioMedical Engineering OnLine, 3*, 9-9. doi:10.1186/1475-925X-3-9

Brigadoi, S., & Cooper, R. J. (2015). How short is short? Optimum source-detector distance for short-separation channels in functional near-infrared spectroscopy. *Neurophotonics, 2*(2), 025005. doi:10.1117/1.NPh.2.2.025005

Center for neuro skills. (n.d.). Frontal lobes. Retrieved from https://www.neuroskills.com/brain-injury/frontal-lobes.php

Chatterjee, S., Phillips, J. P., & Kyriacou, P. A. (2015). Differential pathlength factor estimation for brain-like tissue from a single-layer Monte Carlo model. *Conf Proc IEEE Eng Med Biol Soc, 2015*, 3279-3282. doi:10.1109/EMBC.2015.7319092

Cherian, S. (2016). What you need to know about transimpedance amplifiers – part 1. Retrieved from https://e2e.ti.com/blogs_/b/analogwire/archive/2016/05/06/what-you-need-to-know-about-transimpedance-amplifiers-part-1

Cherry, K. (2018). A Guide to the Anatomy of the Brain. Retrieved from https://www.verywellmind.com/the-anatomy-of-the-brain-2794895

Choi, J.-H., & Loftness, V. (2012). Investigation of human body skin temperatures as a bio-signal to indicate overall thermal sensations. *Building and Environment, 58*, 258-269. doi:https://doi.org/10.1016/j.buildenv.2012.07.003

Cipolla, M. J. (2009). *The Cerebral Circulation*: Morgan & Claypool Life Sciences.

Clark, J. (2016). THE BEER-LAMBERT LAW. Retrieved from http://www.chemguide.co.uk/analysis/uvvisible/beerlambert.html

Cutini, S., & Brigadoi, S. (2014). Unleashing the future potential of functional near-infrared spectroscopy in brain sciences. *Journal of Neuroscience Methods, 232*, 152-156. doi:https://doi.org/10.1016/j.jneumeth.2014.05.024

Dahl, Ø. N. (2013). What is a Diode? Retrieved from https://www.build-electronic-circuits.com/what-is-a-diode/

Dahlitz, M. (2017). Prefrontal Cortex. Retrieved from https://www.neuropsychotherapist.com/prefrontal-cortex/

Davies, D. J., Clancy, M., Lighter, D., Balanos, G. M., Lucas, S. J. E., Dehghani, H., . . . Belli, A. (2017). Frequency-domain vs continuous-wave near-infrared spectroscopy devices: a comparison of clinically viable monitors in controlled hypoxia. *Journal of Clinical Monitoring and Computing, 31*(5), 967-974. doi:10.1007/s10877-016-9942-5

Delpy, D. T., Cope, M., van der Zee, P., Arridge, S., Wray, S., & Wyatt, J. (1988). Estimation of optical pathlength through tissue from direct time of flight measurement. *Phys Med Biol, 33*(12), 1433-1442. doi:https://www.ncbi.nlm.nih.gov/pubmed/3237772

Duncan, A., Meek, J. H., Clemence, M., Elwell, C. E., Fallon, P., Tyszczuk, L., . . . Delpy, D. T. (1996). Measurement of cranial optical path length as a function of age using phase resolved near infrared spectroscopy. *Pediatr Res, 39*(5), 889-894. doi:10.1203/00006450-199605000-00025

ElectronicsTutorials. (n.d.-a). Bipolar Transistor. Retrieved from https://www.electronics-tutorials.ws/transistor/tran_1.html

ElectronicsTutorials. (n.d.-b). Types of Capacitor. Retrieved from https://www.electronics-tutorials.ws/capacitor/cap_2.html

Fairchild. (2014). LM78XX/LM78XXA 3-Terminal 1A Positive Voltage Regulator. Retrieved from http://www.farnell.com/datasheets/2287645.pdf?_ga=2.245766788.1476928674.1521631389-127602487.1516187345&_gac=1.117180788.1521631389.CjwKCAjwhcjVBRBHEiwAoDe5x_QpYSsGq6GL6AYagrygVboFfX1EQVmXFPOvXYTBp9oShFPI3KxErRoCLzMQAvD_BwE

Fatmehsari, Y. R. (2015). *Designing and Implementing a Portable Near-Infrared Imaging System for Monitoring of Human's Functional Brain Activity.* (Master of Science), University of Manitoba,

Fraden, J. (2010). *Handbook of Modern Sensors : Physics, Designs, and Applications*. New York, NY, UNITED STATES: Springer.

Future Electronics. (n.d.). What is a Schottky Diode?

Gagnon, L., Cooper, R. J., Yücel, M. A., Perdue, K. L., Greve, D. N., & Boas, D. A. (2012). Short separation channel location impacts the performance of short channel regression in NIRS. *NeuroImage, 59*(3), 2518-2528. doi:https://doi.org/10.1016/j.neuroimage.2011.08.095

Gagnon, L., Perdue, K., Greve, D. N., Goldenholz, D., Kaskhedikar, G., & Boas, D. A. (2011). Improved recovery of the hemodynamic response in diffuse optical imaging using short optode separations and state-space modeling. *NeuroImage, 56*(3), 1362-1371. doi:https://doi.org/10.1016/j.neuroimage.2011.03.001

GS. (n.d.). GD4066B Quad Bilateral Switches.

Hamatatsu. (n.d.). Si photodiode. Retrieved from http://www.hamamatsu.com/jp/en/4001.html

Harvard University. (2008). How Neural Activity Spurs Blood Flow In The Brain. Retrieved from https://www.sciencedaily.com/releases/2008/06/080626100929.htm

Herold, F., Wiegel, P., Scholkmann, F., Thiers, A., Hamacher, D., & Schega, L. (2017). *Functional near-infrared spectroscopy in movement science: a systematic review on cortical activity in postural and walking tasks*.

Horowitz, P., & Hill, W. (2015). *The art of electronics* (3rd ed. ed.). New York: Cambridge University Press.

Ingebrigtsen, R., & Nygaard, K. H. (2016). *Analog elektronikk*. Oslo: R. Ingebrigtsen.

ISS INC. (n.d.). oxiplexts. In.

Izzetoglu, M., Bunce, S., Izzetoglu, K., Onaral, B., & Pourrezaei, a. (2007). Functional brain imaging using near-infrared technology. *Engineering in Medicine and Biology Magazine, IEEE, 26*(4), 38-46. doi:10.1109/MEMB.2007.384094

Jaafar, R., Zahedi, E., & Ali, M. A. M. (2014, 8-10 Dec. 2014). *Definition and comparison of a new vascular index between young healthy and aged subjects.* Paper presented at the 2014 IEEE Conference on Biomedical Engineering and Sciences (IECBES).

Jobsis, F. F. (1977). Noninvasive, infrared monitoring of cerebral and myocardial oxygen sufficiency and circulatory parameters. *Science, 198*(4323), 1264-1267.

Johnson, M. (2003). *Photodetection and measurement : maximizing performance in optical systems*. New York: McGraw-Hill.

Keim, R. (2016). How to Buffer an Op-Amp Output for Higher Current, Part 1. Retrieved from https://www.allaboutcircuits.com/technical-articles/how-to-buffer-an-op-amp-output-for-higher-current-part-1/

Kelley, A. M. (2012). *Condensed-Phase Molecular Spectroscopy and Photophysics (1)*. Somerset: Somerset, US: John Wiley & Sons, Incorporated.

Knopp, M.-J. (1997). Analog switch 4066. Retrieved from https://ist.uwaterloo.ca/~schepers/MJK/4066.html

Koenraadt, K. L. M., Roelofsen, E. G. J., Duysens, J., & Keijsers, N. L. W. (2014). Cortical control of normal gait and precision stepping: An fNIRS study. *NeuroImage, 85*, 415-422. doi:https://doi.org/10.1016/j.neuroimage.2013.04.070

Langeland, T. (2018). Huden. I Store medisinske leksikon. . Retrieved from https://sml.snl.no/huden

León-Carrión, J., & León-Domínguez, U. (2012). *Functional Near-Infrared Spectroscopy (fNIRS): Principles and Neuroscientific Applications*: INTECH Open Access Publisher.

Li, H., Ruan, J., Xie, Z., Wang, H., & Liu, W. (2007). Investigation of the critical geometric characteristics of living human skulls utilising medical image analysis techniques. *International Journal of Vehicle Safety, 2*(4), 345-367. doi:10.1504/ijvs.2007.016747

Lühmann, A. v. (2014). openNIRS Documentation.

Madsen, S. J. (2013). *Optical Methods and Instrumentation in Brain Imaging and Therapy*. In Bioanalysis, Advanced Materials, Methods, and Devices ;, Vol. 3.

Martelli, F., Binzoni, T., Pifferi, A., Spinelli, L., Farina, A., & Torricelli, A. (2016). There's plenty of light at the bottom: statistics of photon penetration depth in random media. *Scientific Reports, 6*, 27057. doi:10.1038/srep27057

MathWorks. Hardware support. Arduino - matlab. Retrieved from https://se.mathworks.com/hardware-support/arduino-matlab.html

Mathworks. (n.d.). Outlier removal using Hampel identifier. Retrieved from https://se.mathworks.com/help/signal/ref/hampel.html?s_tid=doc_ta

McGraw-Hill Concise Encyclopedia of Physics. (2002). Absorption (electromagnetic radiation). Retrieved from https://encyclopedia2.thefreedictionary.com/Absorption+(electromagnetic+radiation)

Mirtaheri, P. (2018, 2018, January 30.). Patient-Centric Engineering in Rehabilitation (PACER)-Project. Retrieved from https://blogg.hioa.no/optisklab/2018/01/30/pacer-project/

Musa, S. M. (2015). *Computational optical biomedical spectroscopy and imaging*. Boca Raton, FL: CRC Press, Taylor & Francis Group.

Nakamura, K., Kurihara, K., Kawaguchi, H., Obata, T., Ito, H., & Okada, E. (2016). Estimation of partial optical path length in the brain in subject-specific head models for near-infrared spectroscopy. *Optical Review, 23*(2), 316-322. doi:10.1007/s10043-016-0179-9

Naseer, N., & Hong, K.-S. (2015). *FNIRS-based brain-computer interfaces: A review*.

Naseer, N., Hong, M. J., & Hong, K.-S. (2014). Online binary decision decoding using functional near-infrared spectroscopy for the development of brain–computer interface. *Experimental Brain Research, 232*(2), 555-564. doi:10.1007/s00221-013-3764-1

Nate. (n.d.). Analog to Digital Conversion. Retrieved from https://learn.sparkfun.com/tutorials/analog-to-digital-conversion

NIRx. (n.d.). functional Near-InfraRed Spectroscopy (fNIRS). Retrieved from http://nirx.net/fnirs-and-nirx/

Nolte, D. D. (2012). *Optical interferometry for biology and medicine*. In Bioanalysis.

O'Haver, T. (2008). Voltage follower with transistor output current booster. Retrieved from https://terpconnect.umd.edu/~toh/ElectroSim/Booster.html

OSA opto light. (2012). OIS-330 IT855. In.

OSI Optoelectronics. (n.d.). Photodiode Characteristics and Applications. Retrieved from http://www.osioptoelectronics.com/application-notes/an-photodiode-parameters-characteristics.pdf

Pasley, B., & Freeman, R. (2008). Neurovascular coupling. *Scholarpedia, 3*, 5340. doi:doi::10.4249/scholarpedia.5340

Paulsen, T. M., & Heir, W. (2009). Les mer om underhuden. Retrieved from https://ndla.no/nb/node/17203?fag=8

Pease, B. (2001). What's All This Transimpedance Amplifier Stuff, Anyhow? (Part 1). Retrieved from http://www.electronicdesign.com/analog/whats-all-transimpedance-amplifier-stuff-anyhow-part-1

Physics and radio electronics. (n.d.). Photodiode. Retrieved from http://www.physics-and-radio-electronics.com/electronic-devices-and-circuits/semiconductor-diodes/photodiodesymboltypes.html

Richards on the brain. (n.d.). Frontal lobes. Retrieved from http://www.richardsonthebrain.com/frontal-lobe/

Rouse, M. (2015). capacitor (capacitance). Retrieved from https://whatis.techtarget.com/definition/capacitor-capacitance

Sato, H., Kiguchi, M., Kawaguchi, F., & Maki, A. (2004). Practicality of wavelength selection to improve signal-to-noise ratio in near-infrared spectroscopy. *NeuroImage, 21*(4), 1554-1562. doi:https://doi.org/10.1016/j.neuroimage.2003.12.017

Sattel, S. (n.d.). What is a Voltage Regulator. Retrieved from https://www.autodesk.com/products/eagle/blog/what-is-a-voltage-regulator/

Scarpa, F., Brigadoi, S., Cutini, S., Scatturin, P., Zorzi, M., Dell'Acqua, R., & Sparacino, G. (2013). A reference-channel based methodology to improve estimation of event-related hemodynamic response from fNIRS measurements. *NeuroImage, 72*, 106-119. doi:https://doi.org/10.1016/j.neuroimage.2013.01.021

Scholkmann, F., Kleiser, S., Metz, A. J., Zimmermann, R., Mata Pavia, J., Wolf, U., & Wolf, M. (2014). A review on continuous wave functional near-infrared spectroscopy and imaging instrumentation and methodology. *NeuroImage, 85*, 6-27. doi:https://doi.org/10.1016/j.neuroimage.2013.05.004

Scholkmann, F., & Wolf, M. (2013). *General equation for the differential pathlength factor of the frontal human head depending on wavelength and age*.

SM. (2018). Getting started with the Arduino/Genuino Zero. Retrieved from https://www.arduino.cc/en/Guide/ArduinoZero

Spring, K. R., Long, J. C., & Davidson, M. W. (n.d.). Avalanche Photodiodes. Retrieved from https://www.olympus-lifescience.com/en/microscope-resource/primer/java/digitalimaging/avalanche/

Suresh, S. (2016). How to use Proteus 8 Professional - a useful tool for electronic engineers. Retrieved from http://www.techulator.com/resources/15432-Proteus-8-Professional-a-useful-tool-for-electronic-engineers.aspx

Texas instruments. (2015a). LM317A 1% Accurate Three-Terminal Adjustable Regulator. Retrieved from http://www.ti.com/lit/ds/symlink/lm317a.pdf

Texas Instruments. (2015b). OPT101 Monolithic Photodiode and Single-Supply Transimpedance Amplifier.

Texas Instruments. (2017). TL07xx Low-Noise JFET-Input Operational Amplifiers.

Torricelli, A., Contini, D., Pifferi, A., Caffini, M., Re, R., Zucchelli, L., & Spinelli, L. (2014). Time domain functional NIRS imaging for human brain mapping. *NeuroImage, 85*, 28-50. doi:https://doi.org/10.1016/j.neuroimage.2013.05.106

Ushio. (2017). Data Sheet L735/805/850-40B32. In.

Vitorio, R., Stuart, S., Rochester, L., Alcock, L., & Pantall, A. (2017). fNIRS response during walking - Artefact or cortical activity? A systematic review. *Neurosci Biobehav Rev, 83*, 160-172. doi:10.1016/j.neubiorev.2017.10.002

von Lühmann, A., Herff, C., Heger, D., & Schultz, T. (2015). Toward a Wireless Open Source Instrument: Functional Near-infrared Spectroscopy in Mobile Neuroergonomics and BCI Applications. *Frontiers in Human Neuroscience, 9*, 617. doi:10.3389/fnhum.2015.00617

Weiss, G. H., Nossal, R., & Bonner, R. F. (1989). Statistics of Penetration Depth of Photons Re-emitted from Irradiated Tissue. *Journal of Modern Optics, 36*(3), 349-359. doi:10.1080/09500348914550381

Øgendal, L. (2017). *Light Scattering Demystified Theory and Practice*. In (pp. 129).

# 8 Attachments